

# MOCCA: A Fast Algorithm for Parallel MRI Reconstruction Using Model Based Coil Calibration

Gerlind Plonka\*    Yannick Riebe\*

October 30, 2024

## Abstract

**Abstract.** We propose a new fast algorithm for simultaneous recovery of the coil sensitivities and of the magnetization image from incomplete Fourier measurements in parallel MRI. Our approach is based on a parameter model for the coil sensitivities using bivariate trigonometric polynomials of small degree. The derived MOCCA algorithm has low computational complexity of  $\mathcal{O}(N_c N^2 \log N)$  for  $N \times N$  images and  $N_c$  coils and achieves very good performance for incomplete MRI data. We present a complete mathematical analysis of the proposed reconstruction method. Further, we show that MOCCA achieves similarly good reconstruction results as ESPIRiT with a considerably smaller numerical effort which is due to the employed parameter model. Our numerical examples show that MOCCA can outperform several other reconstruction methods.

**Key words.** parallel MRI, deconvolution, discrete Fourier transform, bivariate trigonometric polynomials, structured matrices, regularization

**AMS Subject classifications.** 15A18, 15B05, 42A10, 65F10, 65F22, 65T50, 94A08

## 1 Introduction

One of the biggest innovations in magnetic resonance imaging (MRI) within the last years is the concept of parallel MRI. In this setting, the use of multiple receiver coils allows the reconstruction of high-resolution images from undersampled Fourier data such that the acquisition time can be substantially reduced. Assume we have  $N_c$  receiver channels and (incomplete) discrete measurements, so-called  $k$ -space data, on a cartesian grid given in the form

$$y_{\boldsymbol{\nu}}^{(j)} := y^{(j)}\left(\frac{\boldsymbol{\nu}}{N}\right) = \int_{\Omega} s^{(j)}(\mathbf{x}) m(\mathbf{x}) e^{-2\pi i \frac{\boldsymbol{\nu}}{N} \cdot \mathbf{x}} d\mathbf{x} + n^{(j)}\left(\frac{\boldsymbol{\nu}}{N}\right), \quad j = 0, \dots, N_c - 1, \quad (1.1)$$

for  $\boldsymbol{\nu} \in \Lambda_N := \left\{-\frac{N}{2}, \dots, \frac{N}{2} - 1\right\} \times \left\{-\frac{N}{2}, \dots, \frac{N}{2} - 1\right\}$ , with  $N \in 2\mathbb{N}$ , in the  $2D$ -case, and with  $\mathbf{x} = (x_1, x_2)^T$ . Here,  $m$  denotes the complex-valued unknown magnetization image and  $s^{(j)}$  are the complex valued sensitivity profiles of the  $N_c$  individual coils. The signal is disturbed by noise  $n^{(j)}\left(\frac{\boldsymbol{\nu}}{N}\right)$ . Further,  $\Omega \subset \mathbb{R}^2$  is the bounded area of interest. We

---

\*University of Göttingen, Institute for Numerical and Applied Mathematics, Lotzestr. 16-18, 37083 Göttingen, Germany. Email: (plonka,y.riebe)@math.uni-goettingen.de

assume for simplicity that  $\Omega$  is a square centered around zero. To achieve the wanted acceleration of the acquisition time, the goal is to reconstruct the high-resolution magnetization image  $m$  from a subsampled amount of data  $y_{\nu}^{(j)}$ ,  $\nu \in \Lambda_{\mathcal{P}} \subset \Lambda_N$ , thereby exploiting the information from the parallel receiver channels.

Unfortunately, in general, the coil sensitivity functions  $s^{(j)}$  are also not a priori known and have to be recovered from the measured data. Indeed, the acquisition process produces unpredictable correlations between the magnetization image and the coil sensitivities on the one hand and correlations between different coil sensitivities on the other hand such that  $s^{(j)}$  cannot be accurately estimated beforehand. Therefore, the parallel MRI reconstruction problem can be seen as a multi-channel blind deconvolution problem.

## Contributions

In this paper, we present a new **MO**del-based **CO**il **CA**libration (MOCCA) algorithm to reconstruct the coil sensitivities  $s^{(j)}$  and the magnetization image  $m$  from the given (incomplete) measurements. Our new method employs the assumption that the coil sensitivities  $s^{(j)}$  are smooth functions which can be represented using *bivariate trigonometric polynomials of small degree* such that all  $s^{(j)}$  are already determined by a small number of parameters. In other words,  $s^{(j)}$  are assumed to have small support in  $k$ -space. Therefore, our MOCCA algorithm has low computational complexity of  $\mathcal{O}(N_c N^2 \log N)$  to recover both, the sensitivities as well as the discrete  $N \times N$  magnetization image  $m$ . If the employed discrete models for  $s^{(j)}$  and  $m$  (see (2.1)-(2.2) or more generally (2.4) - (2.5)) are exactly satisfied, we can show that the MOCCA algorithm reconstructs  $s^{(j)}$  and  $m$  exactly (up to one unavoidable ambiguity factor). The parameter vectors determining the coil sensitivities  $s^{(j)}$  can be simultaneously computed for all coils by finding the nullspace vector  $\mathbf{c}$  of the so-called "MOCCA-matrix" (see (3.10)), which is constructed from the given  $k$ -space data in the autocalibration signal (ACS) region. If the data satisfy the model, we show that the nullspace of our MOCCA-matrix is of dimension one almost surely, i.e.,  $\mathbf{c}$  is uniquely defined up to one normalization factor.

Our approach is conceptionally different from ESPIRiT [42] and from all other subspace methods, where the sensitivities are computed based on a low-rank assumption of structured  $k$ -space data. This low-rank assumption is not used in our method, instead, we assume that the sensitivities can be well represented by bivariate trigonometric polynomials of small degree.

Starting with the model (2.2), we propose a completely different procedure to compute the coil sensitivities  $s^{(j)}$ . The low complexity of our MOCCA algorithm stems from the fact that all parameters needed to determine the sensitivities can be recovered by computing just one eigenvector of a moderately sized MOCCA-matrix. By contrast, in ESPIRiT [42] and PISCO [26], the low-rank assumption for a structured matrix of  $k$ -space data leads to  $N^2$  separated eigenvalue problems to compute the coil sensitivity vectors  $(s_{\mathbf{n}}^{(j)})_{j=0}^{N_c-1}$  at each pixel  $\mathbf{n}$ . In those methods, even after applying the so-called sum-of-squares (sos) condition  $\|(s_{\mathbf{n}}^{(j)})_{j=0}^{N_c-1}\|_2 = 1$ , the additional problem arises that one needs to find suitable phase factors for each eigenvalue problem to ensure global smoothness of the phase. This problem is entirely avoided in the MOCCA algorithm.

We provide a complete mathematical analysis of the proposed MOCCA reconstruc-

tion algorithm. In the upcoming paper [21], we will give deeper insights into the relation between the model-based reconstruction of coil sensitivities based on trigonometric polynomials in MOCCA and the assumption that the  $k$ -space data satisfy a structured low-rank model as applied e.g. in ESPIRiT [42], SAKE [38] or PISCO [26]. This relation shows that our model assumption is equally suitable. At the same time, the new model allows a significantly faster computation of the sensitivities from the ACS region by the MOCCA algorithm since it requires neither the high effort of computing the coil sensitivities pixel-wise from many eigenvalue problems as in [42, 38, 26] nor has to deal with all additionally arising problems regarding the phase of sensitivity maps.

While we will focus here on modeling the coil sensitivities using bivariate trigonometric polynomials, the approach can be generalized to other expansions into smooth functions as e.g. linear combination of Gaussians, algebraic polynomials or of splines. Moreover, the model can be directly incorporated into a variational minimization approach such that other constraints on  $m$  and  $s^{(j)}$  can be built in.

## Related Work

Parallel magnetic resonance image reconstruction has a long history. One of the most well-known methods is SENSE [34]. While in [34] the sensitivity functions are estimated beforehand, the SENSE-approach is flexible regarding the modeling of sensitivities.

A series of methods in parallel MRI starts directly from a discretized setting as in (2.1), where the given (incomplete) data are thought to be obtained by a discrete Fourier transform of the product of corresponding discrete function values of  $m$  and  $s^{(j)}$ , see e.g. [8, 28, 39, 18, 13, 42, 24]. Corresponding reconstruction algorithms are frequently based on local approximation of unacquired  $k$ -space data, see e.g. [8, 28], or on subspace methods, see in particular [46, 38, 42, 36, 9, 10, 23, 15, 26]. Often, a prediction method for local approximation of unacquired data  $y_{\nu}^{(j)}$  in  $k$ -space is used, which can be interpreted as a local interpolation scheme. This idea had been proposed in GRAPPA [8] and its forerunners SMASH [39, 18] and was developed further in SPIRiT [28]. The main idea is to compute interpolation weights from fully sampled data in the ACS region of the  $k$ -space, which in turn are applied to recover the unacquired  $k$ -space samples. In SPIRiT [28], a self-consistency condition has been introduced to improve this concept. Subspace methods rely on the assumption that a blockwise Hankel matrix constructed from  $k$ -space data has (approximately) low rank. One of the best performing subspace methods is ESPIRiT [42], which is currently widely used. A closely related approach in [26] proposes a nullspace algorithm together with several ideas to accelerate the computational effort. Low rank matrix completion approaches, as [38], however tend to be computationally expensive.

There have been already earlier attempts to apply model-based techniques to recover the sensitivities for parallel MRI reconstruction, see e.g. [29, 45, 37], where it is assumed that the sensitivities can be written as bivariate algebraic polynomials. These ideas strongly differ from our approach regarding the sensitivity model as well as regarding the reconstruction method. In [45, 37], the polynomial coefficients determining the coil sensitivities are computed using a time-consuming optimization method based on alternating minimization.

Besides the above mentioned models, we shortly refer to two further important classes of reconstruction models which have been studied extensively. The introduc-

tion of compressed sensing algorithms led to MRI reconstructions from incomplete data via convex optimization, [27]. Furthermore, the better understanding that the coil sensitivities need to be computed or at least adjusted during the reconstruction process, led to essential improvements based on more sophisticated optimization models for MR imaging, see e.g. [2, 41, 35, 4, 1, 30, 43, 14, 7, 24]. These models employ suitable constraints on the sensitivity functions  $s^{(j)}$  or the magnetization image  $m$ . Furthermore, other sampling grids as e.g. radial sparse MRI [5], or spirals [37] can be incorporated directly into some of these optimization approaches.

Finally, within recent years, deep learning methods conquered the research area, see e.g. [11, 17, 20, 44, 6, 16]. In particular, in [6], the neural network is based on modeling the sensitivities as algebraic polynomials. While achieving very good reconstruction results, these methods, however, still need to be better understood in order to avoid artificial structures which are not due to the data but to the training process, see e.g. [31], Figure 6.

## Organization of the Paper

In Section 2, we introduce the discrete model for the  $k$ -space data on a cartesian grid and the bivariate trigonometric polynomial model for the coil sensitivities  $s^{(j)}$ . We also present a generalized model that allows to incorporate the sum-of-squares (sos) condition, which is usually taken to handle the occurring ambiguities. In Section 3, we introduce the new MOCCA algorithm (see Algorithm 3.2) for parallel MRI reconstruction from incomplete  $k$ -space data. The algorithm consists of two steps. In the first step, the model parameters for the coil sensitivities  $s^{(j)}$  are recovered from the  $k$ -space data in the ACS region by computing the nullspace vector of the MOCCA matrix. In the second step, the magnetization image  $\mathbf{m}$  is computed by solving a least-squares problem. We propose an iterative algorithm (see Algorithm 3.4) which provides a solution with minimal 2-norm. If the incomplete acquired data follow special patterns, we show that the large equation system arising from the least-squares problem to recover  $\mathbf{m}$  falls apart into many small systems, such that the computational effort can be strongly reduced by Algorithm 3.6. The complete MOCCA algorithm has a complexity of  $\mathcal{O}(N_c N^2 \log N)$ . To improve the MOCCA reconstruction result, we propose a nonlinear local smoothing scheme as a post-processing step. In Section 4 we analyze the new MOCCA reconstruction algorithms. We present uniqueness results for the case when the data exactly satisfy the model, show the convergence of the Algorithm 3.4, derive Algorithm 3.6, and provide conditions that guarantee unique solvability of the least-squares problem in the case of subsampled  $k$ -space data. In Section 5, we present some numerical experiments for MRI data. In particular, we compare the reconstruction results of the MOCCA algorithm with several other reconstruction methods. Conclusions are given in Section 6.

## 2 Modeling of Coil Sensitivities and the Discrete Problem in Parallel MRI

Throughout the paper, we restrict ourselves to the 2D-case, while all ideas can be directly transferred to 3D. We assume for simplicity that the measurement data are given on a cartesian grid. More exactly, assume that we have given the data as in (1.1)

for  $\boldsymbol{\nu} \in \Lambda_N$  (or for  $\boldsymbol{\nu}$  from a subset  $\Lambda_{\mathcal{P}}$  of  $\Lambda_N$ ). In other words, the **sampling grid**  $\frac{1}{N}\Lambda_N$  is a cartesian grid of equidistant points in  $[-\frac{1}{2}, \frac{1}{2}]^2$  with cardinality  $N^2$ .

We apply the notation  $\mathbf{y}^{(j)} := (y_{\boldsymbol{\nu}}^{(j)})_{\boldsymbol{\nu} \in \Lambda_N}$  and  $\mathbf{s}^{(j)} := (s_{\mathbf{n}}^{(j)})_{\mathbf{n} \in \Lambda_N} = (s^{(j)}(\mathbf{n}))_{\mathbf{n} \in \Lambda_N}$  for  $j = 0, \dots, N_c - 1$ , and  $\mathbf{m} := (m_{\mathbf{n}})_{\mathbf{n} \in \Lambda_N} = (m(\mathbf{n}))_{\mathbf{n} \in \Lambda_N}$ . Here and throughout the paper, the index set  $\Lambda_N$  corresponding to an  $(N \times N)$ -image is identified with a one-dimensional index set of length  $N^2$  for the vectorized image, if this is more appropriate, which is easily recognized from the context. Discretization of the integral in (1.1) then yields

$$\mathbf{y}^{(j)} = \mathcal{F}(\mathbf{m} \circ \mathbf{s}^{(j)}), \quad j = 0, \dots, N_c - 1. \quad (2.1)$$

Here  $\mathbf{m} \circ \mathbf{s}^{(j)} := (m_{\mathbf{n}} s_{\mathbf{n}}^{(j)})_{\mathbf{n} \in \Lambda_N}$  denotes the pointwise product and  $\mathcal{F}$  denotes the Fourier operator corresponding to the 2D-Fourier transform of  $(N \times N)$ -matrices. For vectorized images  $\mathbf{m} \circ \mathbf{s}^{(j)} := \text{diag}(\mathbf{s}^{(j)}) \mathbf{m} = \text{diag}(\mathbf{m}) \mathbf{s}^{(j)}$ ,  $\mathcal{F} = \mathcal{F}_{N^2} = (\omega_N^{\boldsymbol{\nu} \cdot \mathbf{n}})_{\boldsymbol{\nu}, \mathbf{n} \in \Lambda_N}$  is of size  $N^2 \times N^2$  with  $\omega_N := e^{-2\pi i/N}$  and  $\omega_N^{\boldsymbol{\nu} \cdot \mathbf{n}} = \omega_N^{\nu_1 n_1 + \nu_2 n_2}$  for  $\boldsymbol{\nu} = (\nu_1, \nu_2)$  and  $\mathbf{n} = (n_1, n_2)$ , and can be presented as the Kronecker product of the Fourier matrices  $(\omega_N^{k\ell})_{k, \ell = -\frac{N}{2}}^{\frac{N}{2}-1}$ . Model (2.1) is usually the starting point for subspace methods to reconstruct  $\mathbf{m}$ , see e.g. [8, 28, 38, 42].

## 2.1 Model for Coil Sensitivities

In practice, the coil sensitivities  $s^{(j)}$  are also unknown for  $j = 0, \dots, N_c - 1$ , but we can suppose that these functions are smooth. The idea is now to model the  $s^{(j)}$  such that they can be reconstructed from a small number of parameters. Therefore, we propose to present the coil sensitivities as bivariate trigonometric polynomials, i.e.,  $s^{(j)}$  have small support in  $k$ -space. Let  $\Lambda_L := \{-n, \dots, n\} \times \{-n, \dots, n\}$ , i.e.,  $|\Lambda_L| = L^2$  with  $L = 2n + 1 \ll N$ . Now let

$$s_{\mathbf{n}}^{(j)} := s^{(j)}(\mathbf{n}) = \sum_{\mathbf{r} \in \Lambda_L} c_{\mathbf{r}}^{(j)} \omega_N^{-\mathbf{r} \cdot \mathbf{n}}, \quad j = 0, \dots, N_c - 1, \mathbf{n} \in \Lambda_N. \quad (2.2)$$

In our numerical experiments, it has been sufficient to use  $L = 5$  (or  $L = 7$ ), such that every  $s^{(j)}$  is already determined by 25 (or 49) parameters  $c_{\mathbf{r}}^{(j)}$ . Let  $\mathbf{W} := (\omega_N^{-\mathbf{r} \cdot \mathbf{n}})_{\mathbf{n} \in \Lambda_N, \mathbf{r} \in \Lambda_L}$  denote a partial matrix of the inverse (scaled) Fourier matrix  $N^2 \mathcal{F}^{-1}$  with only  $L^2$  columns corresponding to indices in  $\Lambda_L$ . Then, with  $\mathbf{c}^{(j)} := (c_{\mathbf{r}}^{(j)})_{\mathbf{r} \in \Lambda_L}$ , we obtain

$$\mathbf{s}^{(j)} := (s_{\mathbf{n}}^{(j)})_{\mathbf{n} \in \Lambda_N} = \mathbf{W} \mathbf{c}^{(j)}, \quad j = 0, \dots, N_c - 1. \quad (2.3)$$

In other words, filling up  $(c_{\mathbf{r}}^{(j)})_{\mathbf{r} \in \Lambda_L}$  by zeros to get  $\tilde{\mathbf{c}}^{(j)} = (\tilde{c}_{\mathbf{r}}^{(j)})_{\mathbf{r} \in \Lambda_N}$  with  $\tilde{c}_{\mathbf{r}}^{(j)} = c_{\mathbf{r}}^{(j)}$  for  $\mathbf{r} \in \Lambda_L$  and  $\tilde{c}_{\mathbf{r}}^{(j)} = 0$  otherwise, we have  $\mathbf{s}^{(j)} = N^2 \mathcal{F}^{-1} \tilde{\mathbf{c}}^{(j)}$ .

## 2.2 Acquired $k$ -space Measurements

To accelerate the acquisition time, only a subset of all  $k$ -space measurements  $(y_{\boldsymbol{\nu}}^{(j)})_{\boldsymbol{\nu} \in \Lambda_N}$ ,  $j = 0, \dots, N_c - 1$ , is acquired. As most of the reconstruction methods, we however require complete  $k$ -space measurements within the neighborhood of the  $k$ -space center, see Figure 1. Let  $\Lambda_M$  be a centered  $M \times M$  index set, i.e.,  $\Lambda_M := \{-\lfloor \frac{M}{2} \rfloor, \dots, \lfloor \frac{M-1}{2} \rfloor\} \times \{-\lfloor \frac{M}{2} \rfloor, \dots, \lfloor \frac{M-1}{2} \rfloor\} \subset \Lambda_N$  (with  $\lfloor x \rfloor = \max\{n \in \mathbb{Z} : n \leq x\}$  being the largest integer

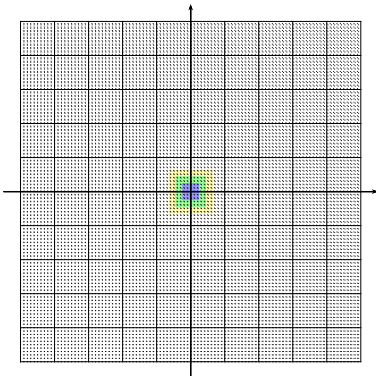


**Figure 1:** Illustration of the grid  $\Lambda_N$  (with  $N = 100$ ), and the subgrids  $\Lambda_L \subset \Lambda_M \subset \Lambda_{M+L-1}$ , the blue subgrid  $\Lambda_L$  (with  $L = 5$ ), the green subgrid  $\Lambda_M$  (with  $M = 9$ ), and the yellow subgrid  $\Lambda_{M+L-1}$ , which needs to be part of the ACS region.

smaller than or equal to  $x$ ). We assume that  $N \gg M \geq L$ , and that the set of  $k$ -space measurements  $\{y_{\nu-\mathbf{r}}^{(j)} : \nu \in \Lambda_M, \mathbf{r} \in \Lambda_L\}$  is completely acquired such that the entries of

$$\mathbf{Y}_{M,L}^{(j)} := (y_{\nu-\mathbf{r}}^{(j)})_{\nu \in \Lambda_M, \mathbf{r} \in \Lambda_L}$$

are well determined for each  $j \in \{0, \dots, N_c - 1\}$ . In other words,  $y_{\nu}^{(j)}$  are assumed to be given for all  $\nu \in \Lambda_{M+L-1} = \{-\lfloor \frac{M}{2} \rfloor - n, \dots, \lfloor \frac{M-1}{2} \rfloor + n\} \times \{-\lfloor \frac{M}{2} \rfloor - n, \dots, \lfloor \frac{M-1}{2} \rfloor + n\}$ , i.e.  $\Lambda_{M+L-1}$  has to be contained in the **autocalibration signal (ACS) region**, see Figure 1.

Beside the measurements from  $\Lambda_{M+L-1}$  we assume that further measurements  $y_{\nu}^{(j)}$  for  $\nu \in \Lambda_N \setminus \Lambda_{M+L-1}$  are acquired, but these measurements may be incomplete. Let  $\mathcal{P}$  denote the projection operator that provides the acquired measurements for each coil. Then

$$\mathcal{P}\mathbf{y}^{(j)} = \mathcal{P}\mathcal{F}(\mathbf{m} \circ \mathbf{s}^{(j)})$$

denote the given measurements for  $j = 0, \dots, N_c - 1$ , where zeros are inserted in case of unacquired data. The subset of  $\Lambda_N$  of indices corresponding to acquired measurements is called  $\Lambda_{\mathcal{P}} \subset \Lambda_N$ .

## 2.3 Problem Statement

Using the discrete model (2.1) together with (2.2), we will solve the following reconstruction problem:

For a given subset  $\mathcal{P}\mathbf{y}^{(j)}$ ,  $j = 0, \dots, N_c - 1$  of  $k$ -space data, find  $\mathbf{m} = (m_{\mathbf{n}})_{\mathbf{n} \in \Lambda_N}$  and the  $N_c$  parameter vectors  $\mathbf{c}^{(j)} = (c_{\mathbf{r}}^{(j)})_{\mathbf{r} \in \Lambda_L} \in \mathbb{C}^{L^2}$  determining  $\mathbf{s}^{(j)}$ ,  $j = 0, \dots, N_c - 1$ , via (2.2).

## 2.4 Generalized Model and Ambiguities

Model (2.2) for the coil sensitivities can simply be generalized to

$$\tilde{s}_{\mathbf{n}}^{(j)} := \gamma_{\mathbf{n}} s_{\mathbf{n}}^{(j)} = \gamma_{\mathbf{n}} \sum_{\mathbf{r} \in \Lambda_L} c_{\mathbf{r}}^{(j)} \omega_N^{-\mathbf{r} \cdot \mathbf{n}} \quad j = 0, \dots, N_c - 1, \mathbf{n} \in \Lambda_N, \quad (2.4)$$

where  $s_{\mathbf{n}}^{(j)}$  in (2.2) is multiplied with the (nonvanishing) sample  $\gamma_{\mathbf{n}} = \gamma(\mathbf{n})$  of a smooth window function  $\gamma$ , and where  $\gamma$  does not depend on  $j$ . Then, (2.1) can be rewritten as

$$\mathbf{y}^{(j)} = \mathcal{F}(\mathbf{m} \circ \mathbf{s}^{(j)}) = \mathcal{F}(\mathbf{m} \circ \gamma^{-1} \circ \gamma \circ \mathbf{s}^{(j)}) = \mathcal{F}(\tilde{\mathbf{m}} \circ \tilde{\mathbf{s}}^{(j)}) \quad (2.5)$$

with  $\gamma := (\gamma_{\mathbf{n}})_{\mathbf{n} \in \Lambda_N}$ ,  $\gamma^{-1} := (\gamma_{\mathbf{n}}^{-1})_{\mathbf{n} \in \Lambda_N}$ ,  $\tilde{\mathbf{s}}^{(j)} := \mathbf{s}^{(j)} \circ \gamma$ , and  $\tilde{\mathbf{m}} := \mathbf{m} \circ \gamma^{-1}$ . In other words, having found  $\mathbf{m}$  and  $\mathbf{s}^{(j)}$ ,  $j = 0, \dots, N_c - 1$ , satisfying (2.1) and (2.2) for all acquired data, we obtain many further solutions  $\tilde{\mathbf{m}}$  and  $\tilde{\mathbf{s}}^{(j)}$  of (2.1), if we apply the more general model (2.4).

Analogously as in [26], Section II, the factors  $\gamma_{\mathbf{n}}$  in (2.4) can be viewed as ambiguity factors. In our "classical" MOCCA model (2.2), this ambiguity problem is resolved by fixing  $\gamma_{\mathbf{n}} = 1$  for  $\mathbf{n} \in \Lambda_N$ , such that  $s_{\mathbf{n}}^{(j)}$  are indeed samples of bivariate trigonometric polynomials. Then we are left with only one global unavoidable ambiguity factor  $\mu \in \mathbb{C} \setminus \{0\}$ , since for obtained  $\mathbf{m}$  and  $\mathbf{s}^{(j)}$  we also find the solution  $\frac{1}{\mu} \mathbf{m}$  and  $\mu \mathbf{s}^{(j)}$ ,  $j = 0, \dots, N_c - 1$ . Applying the generalized model (2.4), the ambiguities arising from the discretization (2.1) will be resolved by employing the sum-of-squares (sos) condition, as in most reconstruction algorithms.

## 2.5 Sum-of-Squares Condition

Many recovery algorithms in parallel MRI (see e.g. [8, 22, 42]) employ the following strategy to recover  $\mathbf{m}$  from the (incomplete) acquired data  $\mathcal{P}\mathbf{y}^{(j)}$ . In a first step, the unacquired  $k$ -space data  $(y_{\nu}^{(j)})_{\nu \in \Lambda_N \setminus \Lambda_{\mathcal{P}}}$  are approximated from the acquired data  $(y_{\nu}^{(j)})_{\nu \in \Lambda_{\mathcal{P}}}$ . Having the complete data  $\mathbf{y}^{(j)}$  in  $k$ -space, one applies the inverse Fourier transform  $\check{\mathbf{y}}^{(j)} = \mathcal{F}^{-1}\mathbf{y}^{(j)}$ ,  $j = 0, \dots, N_c - 1$ , and computes the components  $m_{\mathbf{n}}$  of  $\mathbf{m}$  using the sos condition,

$$m_{\mathbf{n}} := \left( \sum_{j=0}^{N_c-1} |\check{y}_{\mathbf{n}}^{(j)}|^2 \right)^{\frac{1}{2}}, \quad \mathbf{n} \in \Lambda_N. \quad (2.6)$$

At the first glance, this procedure completely disregards the sensitivity vectors  $\mathbf{s}^{(j)}$ . We shortly explain, how (2.6) relates to our setting using the generalized model (2.4). For  $\mathbf{m} = (m_{\mathbf{n}})_{\mathbf{n} \in \Lambda_N}$  and  $\mathbf{s}^{(j)} = (s_{\mathbf{n}}^{(j)})_{\mathbf{n} \in \Lambda_N}$ , satisfying (2.1) and (2.2) for  $j = 0, \dots, N_c - 1$ , we define

$$\gamma_{\mathbf{n}} := \begin{cases} \alpha_{\mathbf{n}} \left( \sum_{j=0}^{N_c-1} |s_{\mathbf{n}}^{(j)}|^2 \right)^{-1/2}, & \mathbf{n} \in \Lambda_N, \sum_{j=0}^{N_c-1} |s_{\mathbf{n}}^{(j)}|^2 > 0, \\ 0 & \text{otherwise,} \end{cases} \quad (2.7)$$

with  $\alpha_{\mathbf{n}} := \text{sign}(m_{\mathbf{n}}) \in \mathbb{C}$  with  $\text{sign}(m_{\mathbf{n}}) := \frac{m_{\mathbf{n}}}{|m_{\mathbf{n}}|}$  for  $|m_{\mathbf{n}}| \neq 0$  and  $\text{sign}(m_{\mathbf{n}}) := 0$  for  $|m_{\mathbf{n}}| = 0$ . Then, we obtain for  $\tilde{\mathbf{s}}^{(j)} = \gamma \circ \mathbf{s}^{(j)} = (\gamma_{\mathbf{n}} s_{\mathbf{n}}^{(j)})_{\mathbf{n} \in \Lambda_N}$  the relation  $\sum_{j=0}^{N_c-1} |\tilde{s}_{\mathbf{n}}^{(j)}|^2 = 1$  for  $\gamma_{\mathbf{n}} \neq 0$ , and  $\sum_{j=0}^{N_c-1} |\tilde{s}_{\mathbf{n}}^{(j)}|^2 = 0$  for  $\gamma_{\mathbf{n}} = 0$ , where  $\tilde{\mathbf{s}}^{(j)}$  satisfies the generalized model (2.4). According to (2.5), we set  $\tilde{m}_{\mathbf{n}} = \frac{1}{\gamma_{\mathbf{n}}} m_{\mathbf{n}}$  for  $\gamma_{\mathbf{n}} \neq 0$  and  $\tilde{m}_{\mathbf{n}} = 0$  for  $\gamma_{\mathbf{n}} = 0$ , such that  $\check{\mathbf{y}}^{(j)} = \mathcal{F}^{-1}\mathbf{y}^{(j)} = \tilde{\mathbf{m}} \circ \tilde{\mathbf{s}}^{(j)}$ . Then we conclude for all  $\mathbf{n} \in \Lambda_N$  with  $\gamma_{\mathbf{n}} \neq 0$

$$\begin{aligned} \tilde{m}_{\mathbf{n}} &= \frac{\text{sign}(m_{\mathbf{n}})|m_{\mathbf{n}}|}{\gamma_{\mathbf{n}}} = \frac{\text{sign}(m_{\mathbf{n}})}{\alpha_{\mathbf{n}}} \left( \sum_{j=0}^{N_c-1} |s_{\mathbf{n}}^{(j)}|^2 \right)^{1/2} |m_{\mathbf{n}}| = |m_{\mathbf{n}}| \left( \sum_{j=0}^{N_c-1} |s_{\mathbf{n}}^{(j)}|^2 \right)^{1/2} \\ &= \left( \sum_{j=0}^{N_c-1} |s_{\mathbf{n}}^{(j)} m_{\mathbf{n}}|^2 \right)^{\frac{1}{2}} = \left( \sum_{j=0}^{N_c-1} |\check{y}_{\mathbf{n}}^{(j)}|^2 \right)^{\frac{1}{2}}. \end{aligned}$$

Hence, the sos solution (2.6) can be obtained from our generalized model (2.4) by choosing  $\gamma_{\mathbf{n}}$  as in (2.7). This observation shows that the application of the sos condition is another way to resolve the ambiguity problem in the discrete parallel MRI setting. Finally, we note that  $m_{\mathbf{n}}$  can only be determined if  $\sum_{j=0}^{N_c-1} |s_{\mathbf{n}}^{(j)}|^2 > 0$ .

**Remark 2.1** *In subspace algorithms as [42] and [26], where the sensitivities are computed from the  $k$ -space data in the ACS region in a first step by solving separate eigenvalue problems at every pixel index  $\mathbf{n}$ , the sos condition is inherently employed by computing normalized eigenvectors  $(s_{\mathbf{n}}^{(j)})_{j=0}^{N_c-1}$ . However, then still the phase factors for every  $\mathbf{n} \in \Lambda_N$  need to be suitably chosen. This problem is avoided in our approach by taking the model (2.2) or (2.4).*

### 3 MOCCA Algorithm for Reconstruction from Incomplete $k$ -space Data

In this section we will derive the MOCCA algorithm that reconstructs  $\mathbf{m} = (m_{\mathbf{n}})_{\mathbf{n} \in \Lambda_N}$  and the sensitivities  $\mathbf{s}^{(j)}$  (which are by (2.2) already determined by  $\mathbf{c}^{(j)} = (c_{\mathbf{r}}^{(j)})_{\mathbf{r} \in \Lambda_L}$ ) from the acquired subset  $\mathcal{P}\mathbf{y}^{(j)}$ ,  $j = 0, \dots, N_c - 1$ . As seen before, (2.1) with (2.2) requires to determine only  $N^2 + L^2 N_c$  parameters. Therefore, we should be able to recover these parameters from incomplete  $k$ -space measurements.

#### 3.1 MOCCA Algorithm

Our approach consists of two steps. First we recover the sensitivities  $\mathbf{s}^{(j)}$  from the acquired  $k$ -space data in the (ACS) region using only the discretization model (2.1) and the sensitivity model (2.2). That is, we have to recover  $\mathbf{c}^{(j)}$ ,  $j = 0, \dots, N_c - 1$ , determining  $\mathbf{s}^{(j)}$  via (2.2). In the second step of the algorithm we will reconstruct  $\mathbf{m}$ .

##### Step 1: Reconstruction of $\mathbf{c}^{(j)}$ .

First, we derive a relation between  $\mathbf{c}^{(j)}$  and the  $k$ -space data  $\mathbf{y}^{(j)}$  that we can apply to recover  $\mathbf{c}^{(j)}$  only from the ACS region.

**Theorem 3.1** *Assume that the vectorized coil sensitivities  $\mathbf{s}^{(j)} \in \mathbb{C}^{N^2}$  satisfy (2.2), i.e.,  $\mathbf{s}^{(j)} = \mathbf{W}\mathbf{c}^{(j)}$  for  $j = 0, \dots, N_c - 1$ , with  $\mathbf{c}^{(j)} \in \mathbb{C}^{L^2}$  as in (2.3). If the model (2.1) is satisfied then*

$$\begin{pmatrix} -\left(\sum_{\substack{\ell=0 \\ \ell \neq 0}}^{N_c-1} \mathbf{Y}_{N,L}^{(\ell)}\right) & \mathbf{Y}_{N,L}^{(0)} & \cdots & \mathbf{Y}_{N,L}^{(0)} \\ \mathbf{Y}_{N,L}^{(1)} & -\left(\sum_{\substack{\ell=0 \\ \ell \neq 1}}^{N_c-1} \mathbf{Y}_{N,L}^{(\ell)}\right) & \cdots & \mathbf{Y}_{N,L}^{(1)} \\ \vdots & & \ddots & \vdots \\ \mathbf{Y}_{N,L}^{(N_c-1)} & \cdots & \mathbf{Y}_{N,L}^{(N_c-1)} & -\left(\sum_{\substack{\ell=0 \\ \ell \neq N_c-1}}^{N_c-1} \mathbf{Y}_{N,L}^{(\ell)}\right) \end{pmatrix} \begin{pmatrix} \mathbf{c}^{(0)} \\ \mathbf{c}^{(1)} \\ \mathbf{c}^{(2)} \\ \vdots \\ \mathbf{c}^{(N_c-1)} \end{pmatrix} = \mathbf{0}, \quad (3.1)$$

where  $\mathbf{Y}_{N,L}^{(j)} := (y_{(\boldsymbol{\nu}-\mathbf{r}) \bmod \Lambda_N}^{(j)})_{\boldsymbol{\nu} \in \Lambda_N, \mathbf{r} \in \Lambda_L} \in \mathbb{C}^{N^2 \times L^2}$ . The matrix in (3.1) is called the MOCCA-matrix  $\mathbf{A}_N \in \mathbb{C}^{N^2 N_c \times L^2 N_c}$ , such that (3.1) reads  $\mathbf{A}_N \mathbf{c} = \mathbf{0}$ .

**Proof:** Model (2.1) together with (2.2) (resp. (2.3)) leads to

$$\check{\mathbf{y}}^{(j)} := \mathcal{F}^{-1} \mathbf{y}^{(j)} = \mathbf{s}^{(j)} \circ \mathbf{m} = \mathbf{m} \circ (\mathbf{W} \mathbf{c}^{(j)}) = (\mathbf{W} \mathbf{c}^{(j)}) \circ \mathbf{m} \quad (3.2)$$

for  $j = 0, \dots, N_c - 1$ . Therefore, we also find

$$\sum_{\substack{\ell=0 \\ \ell \neq j}}^{N_c-1} \check{\mathbf{y}}^{(\ell)} = \sum_{\substack{\ell=0 \\ \ell \neq j}}^{N_c-1} (\mathbf{W} \mathbf{c}^{(\ell)}) \circ \mathbf{m} = (\mathbf{W} \sum_{\substack{\ell=0 \\ \ell \neq j}}^{N_c-1} \mathbf{c}^{(\ell)}) \circ \mathbf{m}$$

and it follows from (3.2) that

$$\begin{aligned} \check{\mathbf{y}}^{(j)} \circ (\mathbf{W} \sum_{\substack{\ell=0 \\ \ell \neq j}}^{N_c-1} \mathbf{c}^{(\ell)}) &= (\mathbf{W} \sum_{\substack{\ell=0 \\ \ell \neq j}}^{N_c-1} \mathbf{c}^{(\ell)}) \circ \check{\mathbf{y}}^{(j)} = (\mathbf{W} \sum_{\substack{\ell=0 \\ \ell \neq j}}^{N_c-1} \mathbf{c}^{(\ell)}) \circ (\mathbf{W} \mathbf{c}^{(j)}) \circ \mathbf{m} \\ &= (\mathbf{W} \sum_{\substack{\ell=0 \\ \ell \neq j}}^{N_c-1} \mathbf{c}^{(\ell)}) \circ \mathbf{m} \circ (\mathbf{W} \mathbf{c}^{(j)}) = (\sum_{\substack{\ell=0 \\ \ell \neq j}}^{N_c-1} \check{\mathbf{y}}^{(\ell)}) \circ (\mathbf{W} \mathbf{c}^{(j)}). \end{aligned} \quad (3.3)$$

This is equivalent with

$$-\text{diag} \left( \sum_{\substack{\ell=0 \\ \ell \neq j}}^{N_c-1} \check{\mathbf{y}}^{(\ell)} \right) \mathbf{W} \mathbf{c}^{(j)} + \text{diag}(\check{\mathbf{y}}^{(j)}) \mathbf{W} \left( \sum_{\substack{\ell=0 \\ \ell \neq j}}^{N_c-1} \mathbf{c}^{(\ell)} \right) = \mathbf{0}, \quad j = 0, \dots, N_c - 1.$$

Application of the 2D-Fourier matrix  $\mathcal{F}$  to the vectorized images yields

$$\left[ -\mathcal{F} \text{diag} \left( \sum_{\substack{\ell=0 \\ \ell \neq j}}^{N_c-1} \check{\mathbf{y}}^{(\ell)} \right) \mathbf{W}, \mathcal{F} \text{diag}(\check{\mathbf{y}}^{(j)}) \mathbf{W} \right] \begin{pmatrix} \mathbf{c}^{(j)} \\ \sum_{\substack{\ell=0 \\ \ell \neq j}}^{N_c-1} \mathbf{c}^{(\ell)} \end{pmatrix} = \mathbf{0}, \quad j = 0, \dots, N_c - 1. \quad (3.4)$$

For the  $\mathbf{r}$ -th column of the matrix  $\mathcal{F} \text{diag}(\check{\mathbf{y}}^{(j)}) \mathbf{W} \in \mathbb{C}^{N^2 \times L^2}$  we observe that

$$\begin{aligned} \mathcal{F} \text{diag}(\check{\mathbf{y}}^{(j)}) (\omega_N^{-\mathbf{n} \cdot \mathbf{r}})_{\mathbf{n} \in \Lambda_N} &= (\omega_N^{\boldsymbol{\nu} \cdot \mathbf{n}})_{\boldsymbol{\nu}, \mathbf{n} \in \Lambda_N} (\omega_N^{-\mathbf{n} \cdot \mathbf{r}} \check{\mathbf{y}}_{\mathbf{n}}^{(j)})_{\mathbf{n} \in \Lambda_N} \\ &= \left( \sum_{\mathbf{n} \in \Lambda_N} \check{\mathbf{y}}_{\mathbf{n}}^{(j)} \omega_N^{\mathbf{n} \cdot (\boldsymbol{\nu} - \mathbf{r})} \right)_{\boldsymbol{\nu} \in \Lambda_N} = (y_{(\boldsymbol{\nu} - \mathbf{r}) \bmod \Lambda_N}^{(j)})_{\boldsymbol{\nu} \in \Lambda_N}. \end{aligned} \quad (3.5)$$

Hence, the  $\boldsymbol{\nu}$ -th row of  $\mathcal{F} \text{diag}(\check{\mathbf{y}}^{(j)}) \mathbf{W}$  contains the  $L^2$  components  $y_{(\boldsymbol{\nu} - \mathbf{r}) \bmod \Lambda_N}^{(j)}$  for  $\mathbf{r} \in \Lambda_L$ , i.e., all components of  $\mathbf{y}^{(j)}$  in the  $(L \times L)$ -block around pixel  $\boldsymbol{\nu}$  in the matrix representation of  $\mathbf{y}^{(j)}$  (using periodic boundary conditions). Thus, (3.4) implies for  $j = 0, \dots, N_c - 1$ ,

$$\left( - \left( \sum_{\substack{\ell=0 \\ \ell \neq j}}^{N_c-1} y_{(\boldsymbol{\nu} - \mathbf{r}) \bmod \Lambda_N}^{(\ell)} \right)_{\boldsymbol{\nu} \in \Lambda_N, \mathbf{r} \in \Lambda_L}, (y_{(\boldsymbol{\nu} - \mathbf{r}) \bmod \Lambda_N}^{(j)})_{\boldsymbol{\nu} \in \Lambda_N, \mathbf{r} \in \Lambda_L} \right) \begin{pmatrix} \mathbf{c}^{(j)} \\ \sum_{\substack{\ell=0 \\ \ell \neq j}}^{N_c-1} \mathbf{c}^{(\ell)} \end{pmatrix} = \mathbf{0}. \quad (3.6)$$

Equivalently, with  $\mathbf{Y}_{N,L}^{(j)} := (y_{(\boldsymbol{\nu} - \mathbf{r}) \bmod \Lambda_N}^{(j)})_{\boldsymbol{\nu} \in \Lambda_N, \mathbf{r} \in \Lambda_L} \in \mathbb{C}^{N^2 \times L^2}$  we obtain (3.1). ■

If the nullspace of  $\mathbf{A}_N$  is one-dimensional, then  $\mathbf{c}$  is uniquely determined up to a global constant. Obviously, it is sufficient to use a much smaller number of rows of the matrix  $\mathbf{A}_N$  above to recover  $\mathbf{c}$ . Therefore, we just need to employ the given  $k$ -space data from the ACS region and consider only the matrix blocks  $\mathbf{Y}_{M,L}^{(j)} :=$

$(y_{(\boldsymbol{\nu}-\mathbf{r})\bmod\Lambda_N}^{(j)})_{\boldsymbol{\nu}\in\Lambda_M, \mathbf{r}\in\Lambda_L} \in \mathbb{C}^{M^2 \times L^2}$ . We construct the MOCCA-matrix  $\mathbf{A}_M \in \mathbb{C}^{M^2 N_c \times L^2 N_c}$  similarly as in (3.1), where the block matrices  $\mathbf{Y}_{N,L}^{(j)}$  are replaced by their submatrices  $\mathbf{Y}_{M,L}^{(j)}$  with only  $M^2$  rows. If the nullspace of  $\mathbf{A}_M$  is still one-dimensional, then  $\mathbf{A}_M \mathbf{c} = \mathbf{0}$  can be solved, and  $\mathbf{c}$  is uniquely determined up to a global (complex) factor. We choose  $\mathbf{c}$  with  $\|\mathbf{c}\|_2 = 1$ . Then, we find the coil sensitivity vectors  $\mathbf{s}^{(j)} = \mathbf{W} \mathbf{c}^{(j)}$ ,  $j = 0, \dots, N_c - 1$ .

**Step 2: Reconstruction of  $\mathbf{m}$ .**

Having determined  $\mathbf{s}^{(j)}$ , we compute  $\mathbf{m}$  using the SENSE approach [34]. In a first step, we normalize  $\mathbf{s}^{(j)}$ . We apply now the generalized model (2.4) and compute  $\tilde{\mathbf{s}}^{(j)} = \boldsymbol{\gamma} \circ \mathbf{s}^{(j)}$  with  $\boldsymbol{\gamma} = (\gamma_{\mathbf{n}})_{\mathbf{n}\in\Lambda_N}$  as in (2.7), where  $\alpha_{\mathbf{n}} := 1$ . We obtain

$$\tilde{s}_{\mathbf{n}}^{(j)} := \begin{cases} \left( \sum_{\ell=0}^{N_c-1} |s_{\mathbf{n}}^{(\ell)}|^2 \right)^{-\frac{1}{2}} s_{\mathbf{n}}^{(j)} & \text{if } \sum_{\ell=0}^{N_c-1} |s_{\mathbf{n}}^{(\ell)}|^2 > \epsilon, \\ 0 & \text{otherwise,} \end{cases} \quad (3.7)$$

where theoretically  $\epsilon = 0$ , and numerically  $\epsilon$  is a small threshold larger than 0. Then, model (2.1) still holds in the form  $\mathbf{y}^{(j)} = \mathcal{F}(\tilde{\mathbf{s}}^{(j)} \circ \tilde{\mathbf{m}})$  for  $j = 0, \dots, N_c - 1$  with  $\tilde{\mathbf{m}} := \boldsymbol{\gamma}^{-1} \circ \mathbf{m}$ . To reconstruct  $\tilde{\mathbf{m}}$ , we solve the minimization problem

$$\tilde{\mathbf{m}} := \operatorname{argmin}_{\mathbf{m} \in \mathbb{C}^{N^2}} \left( \sum_{j=0}^{N_c-1} \|\mathcal{P} \mathbf{y}^{(j)} - (\mathcal{P} \mathcal{F} \operatorname{diag}(\tilde{\mathbf{s}}^{(j)})) \mathbf{m}\|_2^2 \right), \quad (3.8)$$

which leads to the linear system

$$\left( \sum_{j=0}^{N_c-1} (\mathbf{B}^{(j)})^* \mathbf{B}^{(j)} \right) \tilde{\mathbf{m}} = \sum_{j=0}^{N_c-1} (\mathbf{B}^{(j)})^* \mathcal{P} \mathbf{y}^{(j)} \quad (3.9)$$

with  $\mathbf{B}^{(j)} := \mathcal{P} \mathcal{F} \operatorname{diag}(\tilde{\mathbf{s}}^{(j)})$ . Thus,  $\tilde{\mathbf{m}}$  is uniquely determined if the positive semidefinite coefficient matrix  $\sum_{j=0}^{N_c-1} (\mathbf{B}^{(j)})^* \mathbf{B}^{(j)}$  is invertible. The obtained solution set  $(\tilde{\mathbf{m}}, \tilde{\mathbf{s}}^{(j)})$  with  $\tilde{\mathbf{s}}^{(j)}$  in (3.7) and  $\tilde{\mathbf{m}}$  in (3.8) now refers to the generalized coil sensitivity model (2.4) (with  $\boldsymbol{\gamma}$  as in (2.7) and  $\alpha_{\mathbf{n}} = 1$ ), while the solution set  $(\mathbf{m}, \mathbf{s}^{(j)})$  with  $\mathbf{m} = \boldsymbol{\gamma} \circ \tilde{\mathbf{m}}$  refers to (2.2). Replacing now the components of  $\tilde{\mathbf{m}}$  by its modulus,  $|\tilde{\mathbf{m}}| := (|\tilde{m}_{\mathbf{n}}|)_{\mathbf{n}\in\Lambda_N}$ , is equivalent with replacing the coefficients  $\alpha_{\mathbf{n}} = 1$  by  $\alpha_{\mathbf{n}} = \operatorname{sign}(m_{\mathbf{n}})$  as in (2.5), such that the resulting solution  $|\tilde{\mathbf{m}}|$  satisfies the sos condition (2.6). Finally, there is still one ambiguity, which can be used to normalize the image  $\tilde{\mathbf{m}}$ .

The complete reconstruction algorithm to compute  $(\tilde{\mathbf{m}}, \tilde{\mathbf{s}}^{(j)})$  is summarized in Algorithm 3.2.

**Algorithm 3.2** [MOCCA algorithm for reconstruction of  $\mathbf{m}$  and  $\mathbf{s}^{(j)}$ ]

**Input:** Incomplete  $k$ -space data  $\mathcal{P} \mathbf{y}^{(j)}$ ,  $j = 0, \dots, N_c - 1$ , with  $(\mathcal{P} \mathbf{y}^{(j)})_{\boldsymbol{\nu}} = y_{\boldsymbol{\nu}}^{(j)}$  for  $\boldsymbol{\nu} \in \Lambda_{\mathcal{P}}$  and  $(\mathcal{P} \mathbf{y}^{(j)})_{\boldsymbol{\nu}} = 0$  for  $\boldsymbol{\nu} \in \Lambda_N \setminus \Lambda_{\mathcal{P}}$ .

$L = 2n + 1$  determining the support of the trig. polynomials  $s^{(j)}$  in (2.2) in  $k$ -space.

$\Lambda_{M+L-1} \subset \Lambda_{\mathcal{P}} \subset \Lambda_N$ , where  $M \geq L$ . Regularization parameter  $\beta \geq 0$ .

1. Build the matrices  $\mathbf{Y}_{M,L}^{(j)} := (y_{(\nu-\mathbf{r}) \bmod \Lambda_N}^{(j)})_{\nu \in \Lambda_M, \mathbf{r} \in \Lambda_L}$ ,  $j = 0, \dots, N_c - 1$ , and

$$\mathbf{A}_M := \begin{pmatrix} -\left(\sum_{\substack{\ell=0 \\ \ell \neq 0}}^{N_c-1} \mathbf{Y}_{M,L}^{(\ell)}\right) & \mathbf{Y}_{M,L}^{(0)} & \cdots & \mathbf{Y}_{M,L}^{(0)} \\ \mathbf{Y}_{M,L}^{(1)} & -\left(\sum_{\substack{\ell=0 \\ \ell \neq 1}}^{N_c-1} \mathbf{Y}_{M,L}^{(\ell)}\right) & \cdots & \mathbf{Y}_{M,L}^{(1)} \\ \vdots & & \ddots & \vdots \\ \mathbf{Y}_{M,L}^{(N_c-1)} & \cdots & \mathbf{Y}_{M,L}^{(N_c-1)} & -\left(\sum_{\substack{\ell=0 \\ \ell \neq N_c-1}}^{N_c-1} \mathbf{Y}_{M,L}^{(\ell)}\right) \end{pmatrix}. \quad (3.10)$$

2. Compute a singular vector  $\mathbf{c} \in \mathbb{C}^{N_c L^2}$  of  $\mathbf{A}_M$  of norm 1 corresponding to the smallest singular value of  $\mathbf{A}_M$ .
3. Extract the vectors  $\mathbf{c}^{(j)}$ , from  $\mathbf{c} = ((\mathbf{c}^{(0)})^T, (\mathbf{c}^{(1)})^T, \dots, (\mathbf{c}^{(N_c-1)})^T)^T$ . Compute  $\mathbf{s}^{(j)} = \mathbf{W} \mathbf{c}^{(j)}$ ,  $j = 0, \dots, N_c - 1$  by FFT, where  $\mathbf{W} := (\omega_N^{-\mathbf{n} \cdot \mathbf{r}})_{\mathbf{n} \in \Lambda_N, \mathbf{r} \in \Lambda_L}$ .
4. Compute  $\mathbf{d} = (d_{\mathbf{n}})_{\mathbf{n} \in \Lambda_N} := \sum_{j=0}^{N_c-1} \overline{\mathbf{s}^{(j)}} \circ \mathbf{s}^{(j)}$ , where  $\circ$  is the pointwise product. Set  $\mathbf{d}^+ = (d_{\mathbf{n}}^+)_{\mathbf{n} \in \Lambda_N}$  with  $d_{\mathbf{n}}^+ := \frac{1}{d_{\mathbf{n}}}$  for  $|d_{\mathbf{n}}| > \epsilon$  and  $d_{\mathbf{n}}^+ = 0$  otherwise.
5. For  $j = 0 : N_c - 1$  compute  $\tilde{\mathbf{s}}^{(j)} := (\mathbf{d}^+)^{\frac{1}{2}} \circ \mathbf{s}^{(j)} = (\sqrt{d_{\mathbf{n}}^+} s_{\mathbf{n}}^{(j)})_{\mathbf{n} \in \Lambda_N}$ .
6. Solve the equation system

$$\left(\beta \mathbf{I} + \sum_{j=0}^{N_c-1} (\mathbf{B}^{(j)})^* \mathbf{B}^{(j)}\right) \tilde{\mathbf{m}} = \sum_{j=0}^{N_c-1} (\mathbf{B}^{(j)})^* \mathcal{P} \mathbf{y}^{(j)} \quad (3.11)$$

with  $\mathbf{B}^{(j)} := \mathcal{P} \mathcal{F} \text{diag}(\tilde{\mathbf{s}}^{(j)})$ , either iteratively or directly, to compute  $\tilde{\mathbf{m}}$ .

7. Set  $\tilde{\mathbf{s}}^{(j)} := (\text{sign}(\tilde{m}_{\mathbf{n}}) \tilde{s}_{\mathbf{n}}^{(j)})_{\mathbf{n} \in \Lambda_N}$  for  $j = 0, \dots, N_c - 1$  and  $\tilde{\mathbf{m}} := (|\tilde{m}_{\mathbf{n}}|)_{\mathbf{n} \in \Lambda_N}$ .

**Output:**  $(\tilde{\mathbf{m}}, \tilde{\mathbf{s}}^{(j)})$ ,  $j = 0, \dots, N_c - 1$  satisfying (2.4), (2.5), and (2.6).

**Remark 3.3** 1. To compute the singular vector to the smallest singular value  $\sigma_{\min}$  of  $\mathbf{A}_M$  one can employ an inverse power iteration to  $\mathbf{A}_M^* \mathbf{A}_M$  which converges fast in our case.

2. Beside the MOCCA matrix  $\mathbf{A}_M$  in (3.10), there exist many other matrices that serve the same purpose to determine the vectors  $\mathbf{c} = (\mathbf{c}^{(j)})_{j=0}^{N_c-1}$ . Taking for example

$$\mathbf{A}_{M,0} := \begin{pmatrix} -\mathbf{Y}_{M,L}^{(1)} & \mathbf{Y}_{M,L}^{(0)} & \mathbf{0} & \cdots & \mathbf{0} \\ \mathbf{0} & -\mathbf{Y}_{M,L}^{(2)} & \mathbf{Y}_{M,L}^{(1)} & \cdots & \mathbf{0} \\ \vdots & & & \ddots & \vdots \\ \mathbf{Y}_{M,L}^{(N_c-1)} & \cdots & \mathbf{0} & \mathbf{0} & -\mathbf{Y}_{M,L}^{(0)} \end{pmatrix},$$

we conclude similarly as in (3.3) that  $\mathbf{A}_{M,0} \mathbf{c} = \mathbf{0}$ .

3. Relations of the type  $\check{\mathbf{y}}^{(j)} \circ \mathbf{s}^{(\ell)} - \check{\mathbf{y}}^{(\ell)} \circ \mathbf{s}^{(j)} = \mathbf{0}$  for  $j, \ell \in \{0, \dots, N_c - 1\}$  have been used also in other papers, see e.g. [12]. But without using a suitable model for  $\mathbf{s}^{(j)}$ , these relations are not sufficient to derive a reconstruction method for  $\mathbf{s}^{(j)}$ .

4. Note that for the special case  $\Lambda_{\mathcal{P}} = \Lambda_N$  (completely acquired  $k$ -space data), the coefficient matrix of the system (3.11) simplifies to

$$\sum_{j=0}^{N_c-1} (\mathbf{B}^{(j)})^* \mathbf{B}^{(j)} = \sum_{j=0}^{N_c-1} \text{diag}(\tilde{\mathbf{s}}^{(j)})^* \mathcal{F}^* \mathcal{F} \text{diag}(\tilde{\mathbf{s}}^{(j)}) = N^2 \sum_{j=0}^{N_c-1} \text{diag}(\tilde{\mathbf{s}}^{(j)})^* \text{diag}(\tilde{\mathbf{s}}^{(j)}) = N^2 \mathbf{I}_{N^2},$$

such that  $\mathbf{m} = \frac{1}{N^2} \sum_{j=0}^{N_c-1} \text{diag}(\tilde{\mathbf{s}}^{(j)})^* \mathcal{F}^* \mathbf{y}^{(j)} = \sum_{j=0}^{N_c-1} \text{diag}(\tilde{\mathbf{s}}^{(j)})^* \check{\mathbf{y}}^{(j)}$ .

5. To improve the condition number of the coefficient matrix in (3.9), it can be replaced by the positive definite matrix  $\beta \mathbf{I} + \sum_{j=0}^{N_c-1} (\mathbf{B}^{(j)})^* \mathbf{B}^{(j)}$  with small  $\beta > 0$  and the identity matrix  $\mathbf{I}$  of size  $N^2 \times N^2$ . This regularization is often used for least square methods, see e.g. [28].

6. In step 2 of the MOCCA algorithm to reconstruct the magnetization image  $\mathbf{m}$  the least squares problem (3.8) can be simply extended by incorporating a further regularization term for  $\mathbf{m}$  and considering instead the minimization problem

$$\tilde{\mathbf{m}} = \underset{\mathbf{m} \in \mathbb{C}^{N^2}}{\text{argmin}} \left( \sum_{j=0}^{N_c-1} \frac{1}{2} \|\mathcal{P} \mathbf{y}^{(j)} - (\mathcal{P} \mathcal{F} \text{diag}(\tilde{\mathbf{s}}^{(j)})) \mathbf{m}\|_2^2 + \lambda \Phi(\mathbf{m}) \right). \quad (3.12)$$

Here,  $\Phi(\mathbf{m})$  denotes a suitable constraint on the image  $\mathbf{m}$ , and  $\lambda > 0$  is the regularization parameter. As usual in image processing applications, we can for example force that  $\mathbf{m}$  has a sparse representation in a suitably chosen transformed domain, i.e.,  $\Phi(\mathbf{m}) := \|\mathbf{T}\mathbf{m}\|_1$ , where  $\mathbf{T}$  denotes the transform matrix and  $\|\cdot\|_1$  is the usual 1-norm of a vector. Note that in [19], actually two regularization functionals for  $\mathbf{m}$  have been proposed, including the total variation regularization. In [25], a Haar-framelet based transform matrix has been constructed. Both approaches are computationally rather expensive compared to solving (3.8).

7. Note again that the solution ambiguities presented in Section 2.4 are here resolved by employing the sos condition, i.e., by normalizing the sensitivities in step 5 of Algorithm 3.2. Furthermore the remaining global ambiguity and the phase ambiguities (see  $\alpha_{\mathbf{n}}$  in (2.7)) are fixed by choosing  $\mathbf{m}$  with  $\|\mathbf{m}\|_2 = 1$  and with nonnegative real entries. This choice is taken, since the result is later compared with the "ground truth" image obtained from (2.6).

## 3.2 Complexity of the MOCCA Algorithm

Algorithm 3.2 requires  $\mathcal{O}(N_c N^2 \log N)$  operations. In step 2, the singular vector corresponding to the smallest singular value of the MOCCA matrix  $\mathbf{A}_M$  can be obtained by an SVD of  $\mathbf{A}_M$  with at most  $\mathcal{O}((N_c M^2)^2 N_c L^2)$  operations (disregarding the block Hankel structure of  $\mathbf{A}_M$ ). We can assume here that  $N_c M^2 L < \mathcal{O}(N \log N)$  such that this effort is less than  $\mathcal{O}(N_c N^2 \log N)$ . As we will see in the numerical experiments, small numbers  $L$  and  $M$  can be chosen, e.g.  $L = 5$  and  $M = 20$  such that the needed ACS region is covered by 24 ACS lines. The  $N_c$  matrix-vector multiplications in step 3 require  $\mathcal{O}(N_c N^2 L^2)$  operations. Step 4 needs  $\mathcal{O}(N_c N^2)$  operations. Finally, step 5 is the most expensive step, since it requires to solve a large linear system. However, for regular sampling patterns  $\mathcal{P}$  usually taken in parallel MRI (e.g. each second, third, or fourth row/column is acquired), the structure of the coefficient matrix can be employed to derive fast solvers with  $\mathcal{O}(N_c N^2 \log N)$  operations, see Section 3.3.2. Furthermore, in Section 3.3.1 we propose an iterative algorithm to solve (3.11) efficiently.

### 3.3 Efficient Solution of the Least-Squares Problem

Note that the coefficient matrix  $\beta \mathbf{I} + \sum_{j=0}^{N_c-1} (\mathbf{B}^{(j)})^* \mathbf{B}^{(j)}$  (with  $\beta \geq 0$ ) in (3.11) is of size  $N^2 \times N^2$ . Therefore, despite its special structure, it is very large for large  $N$ . To solve (3.11) efficiently, we propose an iterative algorithm and a direct algorithm, where the latter one can be applied in case of structured acquired data.

#### 3.3.1 Weighted Jacobi-Richardson Iteration

We propose the following simple iteration algorithm to solve (3.11).

**Algorithm 3.4** [Weighted Jacobi-Richardson iteration for (3.11)]

**Input:**  $\mathcal{P} \mathbf{y}^{(j)}$  and  $\tilde{\mathbf{s}}^{(j)}$ ,  $j = 0, \dots, N_c - 1$ , from step 2 of Algorithm 3.2,  $\epsilon > 0$ ,  $\beta \geq 0$ .

1. Set  $\tilde{\mathbf{m}}_{-1} := \mathbf{0} \in \mathbb{C}^{N^2}$ ,  $\mathbf{y}_0^{(j)} := \mathcal{P} \mathbf{y}^{(j)}$  and  $\kappa := 0$ .

$$\text{Compute } \tilde{\mathbf{m}}_0 := \sum_{j=0}^{N_c-1} \overline{\tilde{\mathbf{s}}^{(j)}} \circ \mathcal{F}^{-1} \mathbf{y}_0^{(j)}.$$

2. While  $\|\tilde{\mathbf{m}}_\kappa - \tilde{\mathbf{m}}_{\kappa-1}\|_\infty > \epsilon$  do  
Compute

$$\mathbf{y}_{\kappa+1}^{(j)} := \left( \left(1 - \frac{\beta}{N^2}\right) \mathbf{I} - \mathcal{P} \right) \mathcal{F}(\tilde{\mathbf{s}}^{(j)} \circ \tilde{\mathbf{m}}_\kappa) + \mathbf{y}_0^{(j)}, \quad j = 0, \dots, N_c - 1,$$

$$\tilde{\mathbf{m}}_{\kappa+1} := \sum_{j=0}^{N_c-1} \overline{\tilde{\mathbf{s}}^{(j)}} \circ (\mathcal{F}^{-1} \mathbf{y}_{\kappa+1}^{(j)}),$$

and set  $\kappa := \kappa + 1$ .

3. Set  $\tilde{\mathbf{m}} := \tilde{\mathbf{m}}_\kappa$ .

**Output:**  $\tilde{\mathbf{m}}$  solving the system (3.11).

Each iteration step to compute an improved approximation  $\tilde{\mathbf{m}}_\kappa$  in Algorithm 3.4 requires  $\mathcal{O}(N_c N^2 \log N)$  operations for the needed discrete 2D-Fourier transforms. Thus, this system can be solved efficiently. In our numerical experiments in Section 5, we need for example 12 iteration steps for the case if outside the ACS region each second column of data is missing. We will show in Section 4.2 that Algorithm 3.4 always converges, even if the matrix  $\sum_{j=0}^{N_c-1} (\mathbf{B}^{(j)})^* \mathbf{B}^{(j)}$  is not invertible and  $\beta = 0$ . Assuming that the model (2.1) is satisfied, the iteration of Algorithm 3.4 then leads to a solution  $\tilde{\mathbf{m}}$  with minimal norm, see Theorem 4.4.

**Remark 3.5** Algorithm 3.4 can be interpreted as a weighted Jacobi (Richardson) iteration, or as an alternating projection iteration, see Theorem 4.4. Note that the normalization of the sensitivities is essential for a fast convergence of this iteration scheme. In Algorithm 3.4, we iteratively compute the vectors  $\mathbf{y}_{\kappa+1}^{(j)}$ , which can be understood as approximations of the  $k$ -space vectors  $\mathbf{y}^{(j)}$ . In other words, the algorithm provides approximations of the unacquired measurements  $y_{\mathbf{n}}^{(j)}$  for  $\mathbf{n} \in \Lambda_N \setminus \Lambda_{\mathcal{P}}$ . Each further iteration step provides more detail while the image "loses" smoothness. By contrast to other algorithms for parallel MRI based on local interpolation of  $k$ -space data,

as e.g. GRAPPA [8], these approximations depend on all acquired data  $\mathbf{y}_{\mathbf{n}}^{(j)}$  for  $\mathbf{n} \in \Lambda_{\mathcal{P}}$ ,  $j = 0, \dots, N_c - 1$ . Of course, Algorithm 3.4 for (3.11) can be replaced by another iterative solver, as e.g. a cg-solver. In the MR literature, such iterative solvers are usually called iterative SENSE methods. For accelerated convergence in Algorithm 3.4, one can employ an Alternating Anderson–Richardson method, [40].

### 3.3.2 Direct Fast Algorithm for Structured Incomplete Data

The computational effort to recover  $\tilde{\mathbf{m}}$  in step 3 of Algorithm 3.2 can be strongly reduced for special patterns of acquired data. Assume for example that  $N$  is a multiple of 8, and  $\Lambda_{\mathcal{P}}$  contains, beside the ACS region  $\Lambda_{L+M-1}$ , acquired  $k$ -space data for each fourth column, i.e.,  $\Lambda_{\mathcal{P}} = \{-\frac{N}{2}, \dots, \frac{N}{2} - 1\} \times \{-\frac{N}{2}, -\frac{N}{2} + 4, \dots, \frac{N}{2} - 8, \frac{N}{2} - 4\} \cup \Lambda_{L+M-1}$ . In this case, the system (3.11) falls apart into  $\frac{N}{4}$  systems of size  $4 \times 4$  to recover  $\mathbf{m}$ . This idea can be easily transferred to other structured projection patterns. The algorithm is summarized in Algorithm 3.6.

**Algorithm 3.6 (Fast direct solution of (3.11))** (if every fourth column of  $\mathbf{y}^{(j)}$  is acquired)

**Input:**  $\mathcal{P}\mathbf{y}^{(j)}$  and  $\tilde{\mathbf{s}}^{(j)}$ ,  $j = 0, \dots, N_c - 1$ , from step 2 of Algorithm 3.2,  $\beta \geq 0$ .

1. Compute the right-hand side of (3.11),  $\mathbf{R} = (r_{k,\ell})_{(k,\ell) \in \Lambda_N} := \sum_{j=0}^{N_c-1} \tilde{\mathbf{s}}^{(j)} \circ \mathcal{F}^{-1}(\mathcal{P}\mathbf{y}^{(j)})$  using 2-D FFTs of size  $N \times N$ .
2. for  $k = -\frac{N}{2} : 1 : \frac{N}{2} - 1$  do
  - for  $\ell = -\frac{N}{8} : 1 : \frac{N}{8} - 1$  do
    - Set  $\tilde{\mathbf{s}}_{k,\ell}^{(j)} := (\tilde{s}_{k,\ell-\frac{3N}{8}}^{(j)}, \tilde{s}_{k,\ell-\frac{N}{8}}^{(j)}, \tilde{s}_{k,\ell+\frac{N}{8}}^{(j)}, \tilde{s}_{k,\ell+\frac{3N}{8}}^{(j)})^T \in \mathbb{C}^4$  for  $j = 0, \dots, N_c - 1$ .
    - Form the matrix  $\mathbf{G}_{k,\ell} := \frac{4\beta}{N^2} \mathbf{I}_4 + \sum_{j=0}^{N_c-1} \tilde{\mathbf{s}}_{k,\ell}^{(j)} (\tilde{\mathbf{s}}_{k,\ell}^{(j)})^T \in \mathbb{C}^{4 \times 4}$ .
    - Form the vector  $\mathbf{b}_{k,\ell} := 4(r_{k,\ell-\frac{3N}{8}}, r_{k,\ell-\frac{N}{8}}, r_{k,\ell+\frac{N}{8}}, r_{k,\ell+\frac{3N}{8}})^T \in \mathbb{C}^4$ .
    - Solve  $\mathbf{G}_{k,\ell} \mathbf{m} = \mathbf{b}_{k,\ell}$  and set  $(\tilde{m}_{k,\ell-\frac{3N}{8}}, \tilde{m}_{k,\ell-\frac{N}{8}}, \tilde{m}_{k,\ell+\frac{N}{8}}, \tilde{m}_{k,\ell+\frac{3N}{8}})^T := \mathbf{m}$ .
    - end (for)
  - end (for)

**Output:**  $\tilde{\mathbf{m}}$  solving the system (3.11).

**Remark 3.7** 1. Having given for example that every second row and every second column is acquired from the  $k$ -space data  $\mathbf{y}^{(j)}$ , i.e.,  $\Lambda_{\mathcal{P}} \subset \{-\frac{N}{2}, -\frac{N}{2} + 2, \dots, \frac{N}{2} - 2\}^2 \cup \Lambda_{M+L-1}$  (where  $N$  is a multiple of 4), then step 2 of Algorithm 3.6 needs to be replaced by

- for  $k = -\frac{N}{4} : 1 : \frac{N}{4} - 1$  do  
 for  $\ell = -\frac{N}{4} : 1 : \frac{N}{4} - 1$  do  
 Set  $\tilde{\mathbf{s}}_{k,\ell}^{(j)} := (\tilde{s}_{k-\frac{N}{4},\ell-\frac{N}{4}}^{(j)}, \tilde{s}_{k-\frac{N}{4},\ell+\frac{N}{4}}^{(j)}, \tilde{s}_{k+\frac{N}{4},\ell-\frac{N}{4}}^{(j)}, \tilde{s}_{k+\frac{N}{4},\ell+\frac{N}{4}}^{(j)})^T \in \mathbb{C}^4$  for  $j = 0, \dots, N_c - 1$ .  
 Form the matrix  $\mathbf{G}_{k,\ell} := \frac{4\beta}{N^2} \mathbf{I}_4 + \sum_{j=0}^{N_c-1} \tilde{\mathbf{s}}_{k,\ell}^{(j)} (\tilde{\mathbf{s}}_{k,\ell}^{(j)})^T \in \mathbb{C}^{4 \times 4}$ .  
 Form the vector  $\mathbf{b}_{k,\ell} := 4(r_{k-\frac{N}{4},\ell-\frac{N}{4}}, r_{k-\frac{N}{4},\ell+\frac{N}{4}}, r_{k+\frac{N}{4},\ell-\frac{N}{4}}, r_{k+\frac{N}{4},\ell+\frac{N}{4}})^T \in \mathbb{C}^4$ .  
 Solve  $\mathbf{G}_{k,\ell} \mathbf{m} = \mathbf{b}_{k,\ell}$ .  
 Set  $(\tilde{m}_{k-\frac{N}{4},\ell-\frac{N}{4}}, \tilde{m}_{k-\frac{N}{4},\ell+\frac{N}{4}}, \tilde{m}_{k+\frac{N}{4},\ell-\frac{N}{4}}, \tilde{m}_{k+\frac{N}{4},\ell+\frac{N}{4}})^T := \mathbf{m}$ .

end (for)  
end (for)

2. *Fast algorithms for special structures of the acquired  $k$ -space data may be of particular interest in the 3D case employing partially parallel acquisition strategies, see [3].*

The first step of Algorithm 3.6 requires  $N_c$  2-D FFTs with an effort of  $\mathcal{O}(N^2 \log N)$  operations. The second step requires to solve  $\frac{N^2}{4}$  linear systems of size  $4 \times 4$ , with  $\mathcal{O}(N^2)$  operations. The theoretical justification of Algorithm 3.6 is provided in Section 4.3.

### 3.4 Nonlinear Local Smoothing

As a post-processing step, we use a local nonlinear smoothing scheme as proposed e.g. in [32]. To every value  $m_{\mathbf{n}}$ ,  $\mathbf{n} \in \Lambda_N$ , of the reconstructed magnetization image we apply the following procedure,

$$m_{\mathbf{n}}^s := m_{\mathbf{n}} + \tau_{\mathbf{n}} \sum_{\mathbf{r} \in (\Lambda_1 \setminus \{\mathbf{0}\}) \cap \Lambda_N} \frac{g(|m_{\mathbf{n}} - m_{\mathbf{n}-\mathbf{r}}|)}{\|\mathbf{n} - \mathbf{r}\|^2} (m_{\mathbf{n}-\mathbf{r}} - m_{\mathbf{n}}),$$

where  $\Lambda_1 := \{-1, 0, 1\} \times \{-1, 0, 1\}$ ,  $\tau_{\mathbf{n}} := (\sum_{\mathbf{r} \in (\Lambda_1 \setminus \{\mathbf{0}\}) \cap \Lambda_N} \frac{1}{\|\mathbf{n}-\mathbf{r}\|^2})^{-1}$ , and with a function  $g$  which is a so-called diffusivity function. In our experiments, we have applied the Perona-Malik diffusivity  $g(s) = \frac{1}{1+s^2/\lambda}$  with  $\lambda$  as given in Section 5. This procedure is only one step of the smoothing algorithm in [32], which can be interpreted as a discretized nonlinear diffusion smoothing.

## 4 Theoretical Background of Algorithms 3.2-3.6

In this section we show that the MOCCA algorithm almost surely provides a unique reconstruction of the sensitivities  $\mathbf{s}^{(j)}$  (up to an unavoidable global ambiguity factor) if the data  $\mathbf{y}^{(j)}$  satisfy models (2.1)-(2.2) or (2.4)-(2.5), i.e., if  $s_{\mathbf{n}}^{(j)}$  can be represented by trigonometric polynomials of small degree. In Subsection 4.2 we show that the iterative Algorithm 3.4 always converges and yields a solution image  $\tilde{\mathbf{m}}$  with minimal Frobenius norm, if the coefficient matrix occurring in the least squares system (3.11) (with  $\beta = 0$ ) is not invertible. Finally, in Subsection 4.3 we provide a derivation of the fast Algorithm 3.6 and present simple conditions ensuring that the coefficient matrix of the system (3.11) (with  $\beta = 0$ ) is invertible.

### 4.1 Analysis of the MOCCA Algorithm 3.4

The MOCCA Algorithm 3.2 gives rise to the following theorem.

**Theorem 4.1** *Let the incomplete  $k$ -space data  $\mathcal{P}\mathbf{y}^{(j)}$  for  $j = 0, \dots, N_c - 1$ , be given, where the index set  $\Lambda_{\mathcal{P}}$  of acquired measurements contains the ACS region, i.e.,  $\Lambda_{M+L-1} \subset \Lambda_{\mathcal{P}} \subset \Lambda_N$ . Let (2.4), (2.5) and the sos condition (2.6) be satisfied for  $\mathbf{y}^{(j)}$ ,  $\tilde{\mathbf{s}}^{(j)}$ ,  $j = 0, \dots, N_c - 1$ , and  $\tilde{\mathbf{m}}$ , and suppose that:*

1. The matrix  $\mathbf{A}_M$  in (3.10) has a nullspace of dimension 1.
2. The matrix  $\sum_{j=0}^{N_c-1} (\mathbf{B}^{(j)})^* \mathbf{B}^{(j)}$  in (3.11) is invertible.

Then  $\tilde{\mathbf{m}}$  and  $\tilde{\mathbf{s}}^{(j)}$ ,  $j = 0, \dots, N_c - 1$ , are uniquely reconstructed from the  $k$ -space data  $\mathcal{P}\mathbf{y}^{(j)}$  by Algorithm 3.2.

**Proof:** Assumption 1 of Theorem 4.1 ensures that we find the nullspace vector  $\mathbf{c}$  and thus the coil sensitivities  $\mathbf{s}^{(j)} = \mathbf{W}\mathbf{c}^{(j)}$  in (2.3) uniquely up to a complex constant in step 2 of Algorithm 3.2. As shown in Section 2.5, condition (2.6) implies (2.7) for the sensitivities in (2.4). Step 4 of Algorithm 3.2 provides normalized sensitivities  $\tilde{\mathbf{s}}^{(j)}$  satisfying  $\sum_{j=0}^{N_c-1} |\tilde{\mathbf{s}}_{\mathbf{n}}^{(j)}|^2 = 1$  (for  $\sum_{j=0}^{N_c-1} |\mathbf{s}_{\mathbf{n}}^{(j)}|^2 \neq 0$ ). Assumption 2 ensures the unique solvability of the system (3.11) to recover  $\tilde{\mathbf{m}}$ . Note that Assumption 2 can only be satisfied if for  $m_{\mathbf{n}} \neq 0$  we have  $\sum_{j=0}^{N_c-1} |\tilde{\mathbf{s}}_{\mathbf{n}}^{(j)}|^2 = 1$ . Finally, according to (2.6),  $\tilde{\mathbf{m}}$  is uniquely defined after transition to the nonnegative real image  $|\tilde{\mathbf{m}}| = (|m_{\mathbf{n}}|)_{\mathbf{n} \in \Lambda_N}$ , and the factors  $\alpha_{\mathbf{n}} = \text{sign}(m_{\mathbf{n}})$  as in (2.7) finally yield the unique sensitivities  $\tilde{\mathbf{s}}^{(j)}$  in (2.4).  $\blacksquare$

The matrices  $\mathbf{B}^{(j)}$  in (3.11) depend only on the coil sensitivities and on the projection operator  $\mathcal{P}$ , i.e., on the number and the distribution of the acquired measurements. We will study the invertibility of  $\sum_{j=0}^{N_c-1} (\mathbf{B}^{(j)})^* \mathbf{B}^{(j)}$  more exactly in Section 4.2.

In this section we focus on investigating the first assumption in Theorem 4.1 that the matrix  $\mathbf{A}_M$  in (3.10) possesses a nullspace of dimension 1.

We start with some notations. For  $\mathbf{m} = (m_{\mathbf{n}})_{\mathbf{n} \in \Lambda_N} \in \mathbb{C}^{N^2}$  denote by

$$S_N(\mathbf{m}) := \{\mathbf{n} \in \Lambda_N, m_{\mathbf{n}} \neq 0\}, \quad N_m := |S_N(\mathbf{m})| \quad (4.1)$$

the index set of nonzero components of  $\mathbf{m}$  and its cardinality. Let  $L = 2n + 1$  as before. For  $\mathbf{c}^{(j)} = (c_{\mathbf{r}}^{(j)})_{\mathbf{r} \in \Lambda_L}$  we define the corresponding bivariate Laurent polynomial

$$c^{(j)}(\mathbf{z}) := \sum_{\mathbf{r} \in \Lambda_L} c_{\mathbf{r}}^{(j)} \mathbf{z}^{\mathbf{r}} = \sum_{r_1=-n}^n \sum_{r_2=-n}^n c_{(r_1, r_2)}^{(j)} z_1^{r_1} z_2^{r_2}, \quad \mathbf{z} \in \mathbb{C}^2, z_1 \neq 0, z_2 \neq 0,$$

with support  $\Lambda_L$ . We say that  $c^{(j)}(\mathbf{z})$  has degree  $2L - 2$ , if the coefficients corresponding to boundary indices of  $\Lambda_L$  do not all vanish, i.e., if

$$\sum_{r_2=-n}^n |c_{(n, r_2)}^{(j)}| > 0, \quad \sum_{r_2=-n}^n |c_{(-n, r_2)}^{(j)}| > 0, \quad \sum_{r_1=-n}^n |c_{(r_1, n)}^{(j)}| > 0, \quad \sum_{r_1=-n}^n |c_{(r_1, -n)}^{(j)}| > 0. \quad (4.2)$$

As shown in Theorem 3.1, (2.1) with (2.2) implies that the matrix  $\mathbf{A}_N$  in (3.11) always possesses a nullspace of dimension at least 1. The next lemma provides necessary and sufficient conditions for vectors in the nullspace of  $\mathbf{A}_N$ . This observation will be useful to show that the nullspace of  $\mathbf{A}_N$  is of dimension 1 almost surely.

**Lemma 4.1** *Let (2.1) with (2.2) be satisfied for  $j = 0, \dots, N_c - 1$  and  $2L < N$ . Assume that  $\mathbf{V}_{\mathbf{m}} := (\omega_N^{-\mathbf{n} \cdot \ell})_{\mathbf{n} \in S_N(\mathbf{m}), \ell \in \Lambda_{2L-1}} \in \mathbb{C}^{N_m \times (2L-1)^2}$ , with  $S_N(\mathbf{m})$  in (4.1) has full rank  $(2L-1)^2$ . Let  $\mathbf{c} := ((\mathbf{c}^{(0)})^T, \dots, (\mathbf{c}^{(N_c-1)})^T)^T \in \mathbb{C}^{N_c L^2}$  with  $\mathbf{c}^{(j)} = (c_{\mathbf{r}}^{(j)})_{\mathbf{r} \in \Lambda_L} \in \mathbb{C}^{L^2}$  and and  $\mathbf{v} = ((\mathbf{v}^{(0)})^T, (\mathbf{v}^{(1)})^T, \dots, (\mathbf{v}^{(N_c-1)})^T)^T$  with  $\mathbf{v}^{(j)} = (v_{\mathbf{r}}^{(j)})_{\mathbf{r} \in \Lambda_L} \in \mathbb{C}^{L^2}$  be two vectors in the nullspace of the matrix  $\mathbf{A}_N$  in (3.1). Then the corresponding bivariate Laurent polynomials  $c^{(j)}(\mathbf{z})$  and  $v^{(j)}(\mathbf{z})$  satisfy for all  $\mathbf{z} \in \mathbb{C}^2$  with  $z_1 \neq 0, z_2 \neq 0$  the relation*

$$c^{(j)}(\mathbf{z}) \sum_{\substack{\ell=0 \\ \ell \neq j}}^{N_c-1} v^{(\ell)}(\mathbf{z}) = v^{(j)}(\mathbf{z}) \sum_{\substack{\ell=0 \\ \ell \neq j}}^{N_c-1} c^{(\ell)}(\mathbf{z}), \quad j = 0, \dots, N_c - 1. \quad (4.3)$$

**Proof:** Recall that the matrices  $\mathbf{Y}_{N,L}^{(j)} = (y_{(\mathbf{v}-\mathbf{r}) \bmod \Lambda_N}^{(j)})_{\mathbf{v} \in \Lambda_N, \mathbf{r} \in \Lambda_L}$  can by (2.1), (3.4) and (3.5) be rewritten as  $\mathbf{Y}_{N,L}^{(j)} = \mathcal{F} \text{diag}(\check{\mathbf{y}}^{(j)}) \mathbf{W} = \mathcal{F} \text{diag}(\mathbf{m} \circ \mathbf{s}^{(j)}) \mathbf{W}$ . By  $\mathbf{s}^{(j)} = \mathbf{W}\mathbf{c}^{(j)}$ , it follows that

$$\mathcal{F}^{-1} \mathbf{Y}_{N,L}^{(j)} \mathbf{v}^{(\ell)} = \text{diag}(\mathbf{m}) ((\mathbf{W}\mathbf{c}^{(j)}) \circ (\mathbf{W}\mathbf{v}^{(\ell)})), \quad j, \ell = 0, \dots, N_c - 1.$$

Thus,  $\mathbf{A}_N \mathbf{v} = \mathbf{0}$  is equivalent to

$$\text{diag}(\mathbf{m}) \left( - \left( \sum_{\substack{\ell=0 \\ \ell \neq j}}^{N_c-1} \mathbf{W}\mathbf{c}^{(\ell)} \right) \circ (\mathbf{W}\mathbf{v}^{(j)}) + (\mathbf{W}\mathbf{c}^{(j)}) \circ \left( \sum_{\substack{\ell=0 \\ \ell \neq j}}^{N_c-1} \mathbf{W}\mathbf{v}^{(\ell)} \right) \right) = \mathbf{0} \quad (4.4)$$

for  $j = 0, \dots, N_c - 1$ . Using the Laurent polynomial notation in Lemma 4.1, we have  $\mathbf{W}\mathbf{c}^{(j)} = (c^{(j)}(\omega_N^{-\mathbf{n}}))_{\mathbf{n} \in \Lambda_N}$  and  $\mathbf{W}\mathbf{v}^{(j)} = (v^{(j)}(\omega_N^{-\mathbf{n}}))_{\mathbf{n} \in \Lambda_N}$ . We conclude from (4.4) that

$$m_{\mathbf{n}} \left( c^{(j)}(\omega_N^{-\mathbf{n}}) \sum_{\substack{\ell=0 \\ \ell \neq j}}^{N_c-1} v^{(\ell)}(\omega_N^{-\mathbf{n}}) - v^{(j)}(\omega_N^{-\mathbf{n}}) \sum_{\substack{\ell=0 \\ \ell \neq j}}^{N_c-1} c^{(\ell)}(\omega_N^{-\mathbf{n}}) \right) = 0 \quad (4.5)$$

for all  $j = 0, \dots, N_c - 1$  and all  $\mathbf{n} \in \Lambda_N$ . Since the Laurent polynomials  $c^{(j)}(\mathbf{z})$  and  $v^{(\ell)}(\mathbf{z})$  are of degree at most  $2(L-1)$ , it follows that the sum  $c^{(j)}(\mathbf{z}) \sum_{\substack{\ell=0 \\ \ell \neq j}}^{N_c-1} v^{(\ell)}(\mathbf{z}) - v^{(j)}(\mathbf{z}) \sum_{\substack{\ell=0 \\ \ell \neq j}}^{N_c-1} c^{(\ell)}(\mathbf{z})$  has at most degree  $4(L-1)$ , and by construction can only have nonzero coefficients corresponding to the index set  $\Lambda_{2L-1}$ . By assumption, we have  $m_{\mathbf{n}} \neq 0$  for all  $\mathbf{n} \in S_N(\mathbf{m})$ , and the matrix  $\mathbf{V}_{\mathbf{m}} := (\omega_N^{-\mathbf{n} \cdot \mathbf{r}})_{\mathbf{n} \in S_N(\mathbf{m}), \mathbf{r} \in \Lambda_{2L-1}}$  has full rank  $(2L-1)^2$ . Therefore, the interpolation conditions in (4.5) imply the condition (4.3). ■

**Theorem 4.2** *Let the assumptions of Lemma 4.1 be satisfied and assume that  $\mathbf{A}_N \mathbf{c} = \mathbf{0}$  with  $\mathbf{c} := ((\mathbf{c}^{(0)})^T, \dots, (\mathbf{c}^{(N_c-1)})^T)^T \in \mathbb{C}^{N_c L^2}$ , where the partial vectors  $\mathbf{c}^{(j)}$  satisfy (4.2). Then  $\mathbf{A}_N$  in (3.1) has a nullspace of dimension 1 almost surely.*

**Proof:** By (3.1), the dimension of the nullspace of  $\mathbf{A}_N$  is at least 1 and we have  $\mathbf{A}_N \mathbf{c} = \mathbf{0}$  with  $\mathbf{c} := ((\mathbf{c}^{(0)})^T, \dots, (\mathbf{c}^{(N_c-1)})^T)^T \in \mathbb{C}^{N_c L^2}$ . By Lemma 4.1, each further vector  $\mathbf{v} = ((\mathbf{v}^{(0)})^T, (\mathbf{v}^{(1)})^T, \dots, (\mathbf{v}^{(N_c-1)})^T)^T$  with  $\mathbf{v}^{(j)} = (v_{\mathbf{r}}^{(j)})_{\mathbf{r} \in \Lambda_L} \in \mathbb{C}^{L^2}$  in the nullspace of  $\mathbf{A}_N$  satisfies (4.3). Condition (4.2) ensures that  $c^{(j)}(\mathbf{z})$ ,  $j = 0, \dots, N_c - 1$ , have full degree  $2(L-1)$ , such that the (bivariate) rational functions  $\sum_{\substack{\ell=0 \\ \ell \neq j}}^{N_c-1} \frac{c^{(\ell)}(\mathbf{z})}{c^{(j)}(\mathbf{z})} = \sum_{\substack{\ell=0 \\ \ell \neq j}}^{N_c-1} \frac{z_1^n z_2^n c^{(\ell)}(\mathbf{z})}{z_1^n z_2^n c^{(j)}(\mathbf{z})}$  are of type  $(2(L-1), 2(L-1))$ . This type is almost surely minimal, i.e.,  $\sum_{\substack{\ell=0 \\ \ell \neq j}}^{N_c-1} z_1^n z_2^n c^{(\ell)}(\mathbf{z})$  and  $z_1^n z_2^n c^{(j)}(\mathbf{z})$  almost surely have no common zeros. For each  $j = 0, \dots, N_c - 1$  we conclude: If  $v^{(j)}(\mathbf{z})$  is not the zero polynomial, then (4.3) implies that

$$\sum_{\substack{\ell=0 \\ \ell \neq j}}^{N_c-1} \frac{c^{(\ell)}(\mathbf{z})}{c^{(j)}(\mathbf{z})} = \sum_{\substack{\ell=0 \\ \ell \neq j}}^{N_c-1} \frac{v^{(\ell)}(\mathbf{z})}{v^{(j)}(\mathbf{z})}$$

almost everywhere, and since  $v^{(j)}(\mathbf{z})$  is by construction a Laurent polynomial of degree at most  $2(L-1)$ , it follows that  $v^{(j)}(\mathbf{z}) = \mu c^{(j)}(\mathbf{z})$  with some global constant  $\mu$  which does not depend on  $j$ . Hence,  $\mathbf{A}_N$  in (3.1) has a nullspace of dimension 1. ■

**Remark 4.3** *The conditions of Lemma 4.1 can be easily satisfied. For example,  $\mathbf{V}_m$  already satisfies the rank assumption, if  $m_n \neq 0$  for  $\mathbf{n} \in \Lambda_{2L-1}$ . If  $m_n = 0$  for some  $\mathbf{n} \in \Lambda_{2L-1}$  then it is sufficient to find an index  $\mathbf{n} + (2L-1)\boldsymbol{\nu} \in \Lambda_N$  with  $m_{\mathbf{n}+(2L-1)\boldsymbol{\nu}} \neq 0$  to satisfy the condition. Therefore, the nullspace condition is satisfied almost surely for  $\mathbf{A}_M$  with  $M \geq 2L$ , if (4.2) holds and if the ACS region is chosen large enough. If (4.2) is not satisfied, this is an indication that  $L$  has been chosen too large in the model (2.2) or the ACS region is too small.*

*In practice, the considered models (2.1) and (2.2) are not exactly satisfied for MRI data, and the matrix  $\mathbf{A}_M$  may have several small singular values of similar size. In this case, a suitable linear combination singular vectors corresponding to these singular values seems to be appropriate such that  $\mathbf{d}$  in step 4 of Algorithm 3.2 is well bounded away from zero, see Section 5.*

## 4.2 Analysis of Algorithm 3.4

In this subsection, we show the convergence of the iteration method in Algorithm 3.4 to a solution of (3.11).

**Theorem 4.4** *If the model assumptions (2.1) and (2.2) are satisfied with  $\sum_{j=0}^{N_c-1} |s_{\mathbf{n}}^{(j)}|^2 > 0$  for all  $\mathbf{n} \in S_N(\mathbf{m})$  in (4.1), then the iteration scheme in Algorithm 3.4 converges for  $0 \leq \beta < N^2$  to a solution  $\tilde{\mathbf{m}}$  of (3.11). In particular, for  $\beta = 0$ , Algorithm 3.4 always converges to a solution with minimal 2-norm.*

**Proof:** 1. We first assume that  $\sum_{j=0}^{N_c-1} |s_{\mathbf{n}}^{(j)}|^2 > 0$  for all  $\mathbf{n} \in \Lambda_N$ . Then the normalized vectors  $\tilde{\mathbf{s}}^{(j)}$  defined in (3.7) satisfy  $\sum_{j=0}^{N_c-1} |\tilde{s}_{\mathbf{n}}^{(j)}|^2 = 1$  for  $\mathbf{n} \in \Lambda_N$ . Since  $\frac{1}{N}\mathcal{F}$  is a unitary matrix, i.e.,  $\mathcal{F}^{-1} = \frac{1}{N^2}\mathcal{F}^*$ , and  $\mathcal{P}$  a projection matrix, we obtain for the largest eigenvalue of the matrix  $\mathbf{Q} := \frac{1}{N^2}(\beta\mathbf{I} + \sum_{j=0}^{N_c-1} (\mathbf{B}^{(j)})^* \mathbf{B}^{(j)})$  with  $\mathbf{B}^{(j)} = \mathcal{P}\mathcal{F}\text{diag}(\tilde{\mathbf{s}}^{(j)})$  that

$$\max_{\substack{\mathbf{w} \in \mathbb{C}^{N^2} \\ \|\mathbf{w}\|_2=1}} \mathbf{w}^* \mathbf{Q} \mathbf{w} = \frac{\beta}{N^2} + \max_{\substack{\mathbf{w} \in \mathbb{C}^{N^2} \\ \|\mathbf{w}\|_2=1}} \sum_{j=0}^{N_c-1} \left\| \frac{1}{N} \mathbf{B}^{(j)} \mathbf{w} \right\|_2^2 = \frac{\beta}{N^2} + \max_{\substack{\mathbf{w} \in \mathbb{C}^{N^2} \\ \|\mathbf{w}\|_2=1}} \sum_{j=0}^{N_c-1} \left\| \mathcal{P} \frac{1}{N} \mathcal{F} \text{diag}(\tilde{\mathbf{s}}^{(j)}) \mathbf{w} \right\|_2^2$$

and therefore

$$\begin{aligned} \max_{\substack{\mathbf{w} \in \mathbb{C}^{N^2} \\ \|\mathbf{w}\|_2=1}} \mathbf{w}^* \mathbf{Q} \mathbf{w} &\leq \frac{\beta}{N^2} + \max_{\substack{\mathbf{w} \in \mathbb{C}^{N^2} \\ \|\mathbf{w}\|_2=1}} \sum_{j=0}^{N_c-1} \left\| \text{diag}(\tilde{\mathbf{s}}^{(j)}) \mathbf{w} \right\|_2^2 = \frac{\beta}{N^2} + \max_{\substack{\mathbf{w} \in \mathbb{C}^{N^2} \\ \|\mathbf{w}\|_2=1}} \sum_{j=0}^{N_c-1} \sum_{\mathbf{n} \in \Lambda_N} |\tilde{s}_{\mathbf{n}}^{(j)}|^2 |w_{\mathbf{n}}|^2 \\ &= \frac{\beta}{N^2} + \max_{\substack{\mathbf{w} \in \mathbb{C}^{N^2} \\ \|\mathbf{w}\|_2=1}} \sum_{\mathbf{n} \in \Lambda_N} \left( \sum_{j=0}^{N_c-1} |\tilde{s}_{\mathbf{n}}^{(j)}|^2 \right) |w_{\mathbf{n}}|^2 = 1 + \frac{\beta}{N^2}. \end{aligned} \quad (4.6)$$

The iteration procedure in step 2 of Algorithm 3.4 implies

$$\begin{aligned} \tilde{\mathbf{m}}_{\kappa+1} &= \left( \sum_{j=0}^{N_c-1} \text{diag}(\tilde{\mathbf{s}}^{(j)})^* \mathcal{F}^{-1} \left( \left( 1 - \frac{\beta}{N^2} \right) \mathbf{I} - \mathcal{P} \right) \mathcal{F} \text{diag}(\tilde{\mathbf{s}}^{(j)}) \right) \tilde{\mathbf{m}}_{\kappa} + \sum_{j=0}^{N_c-1} \text{diag}(\tilde{\mathbf{s}}^{(j)})^* \mathcal{F}^{-1} \mathbf{y}_0^{(j)} \\ &= \left( \left( 1 - \frac{\beta}{N^2} \right) \mathbf{I} - \frac{1}{N^2} \left( \sum_{j=0}^{N_c-1} (\mathbf{B}^{(j)})^* \mathbf{B}^{(j)} \right) \right) \tilde{\mathbf{m}}_{\kappa} + \frac{1}{N^2} \sum_{j=0}^{N_c-1} (\mathbf{B}^{(j)})^* \mathbf{y}_0^{(j)}. \end{aligned} \quad (4.7)$$

Convergence of this iteration scheme is ensured if the spectral radius of the iteration matrix

$$\left(1 - \frac{\beta}{N^2}\right)\mathbf{I} - \frac{1}{N^2} \left( \sum_{j=0}^{N_c-1} (\mathbf{B}^{(j)})^* \mathbf{B}^{(j)} \right) = \mathbf{I} - \mathbf{Q} \quad (4.8)$$

is smaller than 1. The matrix  $\mathbf{Q}$  is by construction positive semidefinite, and by (4.6), all its eigenvalues are in the interval  $[\frac{\beta}{N^2}, 1 + \frac{\beta}{N^2}]$ . Therefore,  $\mathbf{I} - \mathbf{Q}$  has all its eigenvalues in  $[-\frac{\beta}{N^2}, 1 - \frac{\beta}{N^2}]$ .

2. Let  $\mathbf{Q}$  be invertible and  $0 \leq \beta < N^2$ . Then  $\|\mathbf{I} - \mathbf{Q}\|_2 < 1$  and (4.7) converges. Its fixed point satisfies

$$\tilde{\mathbf{m}} = \left( \left(1 - \frac{\beta}{N^2}\right)\mathbf{I} - \frac{1}{N^2} \left( \sum_{j=0}^{N_c-1} (\mathbf{B}^{(j)})^* \mathbf{B}^{(j)} \right) \right) \tilde{\mathbf{m}} + \frac{1}{N^2} \sum_{j=0}^{N_c-1} (\mathbf{B}^{(j)})^* \mathbf{y}_0^{(j)},$$

i.e.,  $(\beta\mathbf{I} + \sum_{j=0}^{N_c-1} (\mathbf{B}^{(j)})^* \mathbf{B}^{(j)}) \tilde{\mathbf{m}} = \sum_{j=0}^{N_c-1} (\mathbf{B}^{(j)})^* \mathbf{y}_0^{(j)}$ .

3. Assume now that  $\mathbf{Q}$  is not invertible, i.e.,  $\beta = 0$  and  $\sum_{j=0}^{N_c-1} (\mathbf{B}^{(j)})^* \mathbf{B}^{(j)}$  is singular. Then from the definitions of  $\mathbf{y}_0^{(j)} = \mathcal{P} \mathbf{y}^{(j)} = \mathcal{P} \mathcal{F} \text{diag}(\tilde{\mathbf{s}}^{(j)}) \tilde{\mathbf{m}} = \mathbf{B}^{(j)} \tilde{\mathbf{m}}$  and of  $\tilde{\mathbf{m}}_0$  in Algorithm 3.4 it follows with  $\mathcal{P} = \mathcal{P}^* = \mathcal{P}^* \mathcal{P}$  that

$$\tilde{\mathbf{m}}_0 = \sum_{j=0}^{N_c-1} \overline{\tilde{\mathbf{s}}^{(j)}} \circ (\mathcal{F}^{-1} \mathbf{y}_0^{(j)}) = \frac{1}{N^2} \sum_{j=0}^{N_c-1} (\mathbf{B}^{(j)})^* \mathbf{y}_0^{(j)} = \frac{1}{N^2} \sum_{j=0}^{N_c-1} (\mathbf{B}^{(j)})^* \mathbf{B}^{(j)} \tilde{\mathbf{m}} = \mathbf{Q} \tilde{\mathbf{m}}$$

is in the image space of  $\mathbf{Q} = \mathbf{Q}^*$  and therefore orthogonal to the nullspace of  $\mathbf{Q}$ . In particular, we conclude that the system (3.11) has always solutions. The iteration scheme (4.7) implies that also each further vector  $\mathbf{m}_\kappa$  is in the image space of  $\mathbf{Q}$ . Restricted to the image space of  $\mathbf{Q}$ , the iteration matrix in (4.7) has again a spectral radius smaller than 1. Hence, the fixed point of (4.7) exists also in this case and is a solution of (3.11). Moreover, this solution is of minimal 2-norm, since it is orthogonal to the nullspace of  $\mathbf{Q}$ .

4. Finally, let  $\Lambda_0 \neq \emptyset$  be the index set with  $\sum_{j=0}^{N_c-1} |s_{\mathbf{n}}^{(j)}|^2 = 0$  for  $\mathbf{n} \in \Lambda_0$ . By assumption,  $\Lambda_0 \cap \mathcal{S}_N(\mathbf{m}) = \emptyset$ . Then the vectors  $\tilde{\mathbf{s}}^{(j)}$ ,  $\mathbf{y}_0^{(j)}$  and  $\tilde{\mathbf{m}}_\kappa$  all have zero components for  $\mathbf{n} \in \Lambda_0$ , the matrices  $\mathbf{B}^{(j)}$  have zero columns, and the matrix  $\mathbf{Q}$  has zero columns and zero rows for all indices  $\mathbf{n} \in \Lambda_0$ . In this case the proof applies as before for the reduced vectors and matrices, where all components of the vectors and all columns or columns/rows of the matrices corresponding to the index set  $\Lambda_0$  are removed. ■

### 4.3 Derivation of Algorithm 3.6 and Unique Solvability of (3.11)

In this section we derive Algorithm 3.6. Furthermore, we study the invertibility of  $\sum_{j=0}^{N_c-1} (\mathbf{B}^{(j)})^* \mathbf{B}^{(j)}$ , which depends on the index set  $\Lambda_{\mathcal{P}} \subset \Lambda_N$  of acquired data.

Assume that we have computed  $\tilde{\mathbf{s}}^{(j)}$ ,  $j = 0, \dots, N_c - 1$ , as in step 5 of Algorithm 3.2. To derive a direct efficient algorithm to solve (3.11), we require some notations. To avoid confusion, in this section, we explicitly distinguish between the  $N \times N$  matrices  $\mathbf{y}^{(j)}$ ,  $\mathbf{s}^{(j)}$ ,  $\tilde{\mathbf{s}}^{(j)}$ ,  $\mathbf{m}$ ,  $\mathcal{P}$  and their columnwise vectorized counterparts  $\text{vec}(\mathbf{y}^{(j)})$ ,  $\text{vec}(\mathbf{s}^{(j)})$ ,  $\text{vec}(\tilde{\mathbf{s}}^{(j)})$ ,  $\text{vec}(\mathbf{m})$ ,  $\text{vec}(\mathcal{P})$  in  $\mathbb{C}^{N^2}$ . The Kronecker product of two  $N \times N$  matrices

$\mathbf{A} = (a_{k,\ell})_{k,\ell=-\frac{N}{2}}^{\frac{N}{2}-1} \in \mathbb{C}^{N \times N}$  and  $\mathbf{B} \in \mathbb{C}^{N \times N}$  is given as

$$\mathbf{A} \otimes \mathbf{B} := (a_{k,\ell} \mathbf{B})_{k,\ell=-\frac{N}{2}}^{\frac{N}{2}-1} \in \mathbb{C}^{N^2 \times N^2}.$$

For properties of the Kronecker product of matrices and the discrete Fourier transform, we refer to Section 3.4 in [33]. In matrix form, the Fourier operator  $\mathcal{F}$  denotes the centered 2D DFT, and in vector form it can be written as  $\mathcal{F} = \mathbf{F}_N \otimes \mathbf{F}_N$ , where  $\mathbf{F}_N = (\omega_N^{k\ell})_{k,\ell=-\frac{N}{2}}^{\frac{N}{2}-1}$  is the (centered) Fourier matrix of size  $N \times N$ , which satisfies  $\mathbf{F}_N^* = N\mathbf{F}_N^{-1}$ . With these notations, (2.1) with incomplete  $k$ -space data has the matrix form

$$\mathcal{P} \circ \mathbf{y}^{(j)} = \mathcal{P} \circ (\mathbf{F}_N(\mathbf{m} \circ \mathbf{s}^{(j)})\mathbf{F}_N)$$

and the vector form  $\text{vec}(\mathcal{P}) \circ \text{vec}(\mathbf{y}^{(j)}) = \text{vec}(\mathcal{P}) \circ (\mathbf{F}_N \otimes \mathbf{F}_N)(\text{vec}(\mathbf{m}) \circ \text{vec}(\mathbf{s}^{(j)}))$ .

We present exemplarily the case, where  $N$  is a multiple of 8, and  $\Lambda_{\mathcal{P}}$  contains beside the ACS region  $\Lambda_{L+M-1}$  the subset  $\Lambda_{\mathcal{P}_1} := \{k : -\frac{N}{2} \leq k \leq \frac{N}{2} - 1\} \times \{4k : -\frac{N}{8} \leq k \leq \frac{N}{8} - 1\}$ , with  $\frac{N^2}{4}$  components, where, besides the ACS region, only every fourth column of the  $N \times N$  image representation  $\mathbf{y}^{(j)}$  is acquired. Let  $\mathcal{P}_1$  denote the corresponding projection matrix, i.e.,  $\mathcal{P}_1 = (p_{k,\ell})_{(k,\ell) \in \Lambda_N}$  with  $p_{k,\ell} = 1$  if  $\ell \equiv 0 \pmod{4}$  and  $p_{k,\ell} = 0$  otherwise. Then  $\text{diag}(\text{vec}(\mathcal{P}_1))$  is of the form

$$\text{diag}(\text{vec}(\mathcal{P}_1)) = \mathbf{P}_1 \otimes \mathbf{I}_N \quad \text{with } \mathbf{P}_1 = \text{diag}((1, 0, 0, 0, 1, 0, 0, 0, \dots, 1, 0, 0, 0)) \in \mathbb{C}^{N \times N},$$

where  $\mathbf{I}_N$  is the  $N \times N$  unitary matrix. For the  $N^2 \times N^2$  coefficient matrix of (3.11),  $\sum_{j=0}^{N_c-1} (\mathbf{B}^{(j)})^* \mathbf{B}^{(j)}$ , we obtain by  $\text{diag}(\text{vec}(\mathcal{P}_1))^* \text{diag}(\text{vec}(\mathcal{P}_1)) = \text{diag}(\text{vec}(\mathcal{P}_1)) = \mathbf{P}_1 \otimes \mathbf{I}_N$

$$\begin{aligned} \sum_{j=0}^{N_c-1} (\mathbf{B}^{(j)})^* \mathbf{B}^{(j)} &= \sum_{j=0}^{N_c-1} \text{diag}(\text{vec}(\tilde{\mathbf{s}}^{(j)}))^* (\mathbf{F}_N \otimes \mathbf{F}_N)^* (\mathbf{P}_1 \otimes \mathbf{I}_N) (\mathbf{F}_N \otimes \mathbf{F}_N) \text{diag}(\text{vec}(\tilde{\mathbf{s}}^{(j)})) \\ &= \sum_{j=0}^{N_c-1} \text{diag}(\text{vec}(\tilde{\mathbf{s}}^{(j)}))^* ((\mathbf{F}_N^* \mathbf{P}_1 \mathbf{F}_N) \otimes (\mathbf{F}_N^* \mathbf{F}_N)) \text{diag}(\text{vec}(\tilde{\mathbf{s}}^{(j)})), \end{aligned}$$

where  $(\mathbf{F}_N)^* \mathbf{F}_N = N\mathbf{I}_N$  and  $(\mathbf{F}_N)^* \mathbf{P}_1 \mathbf{F}_N = \frac{N}{4} (\delta_{k,\ell \pmod{4}})_{k,\ell=-\frac{N}{2}}^{\frac{N}{2}-1} = \frac{N}{4} \mathbf{E}_4 \otimes \mathbf{I}_{\frac{N}{4}}$ , where  $\mathbf{E}_4$  is a  $4 \times 4$  matrix containing only ones. Therefore, using that  $\mathbf{I}_{\frac{N}{4}} \otimes \mathbf{I}_N = \mathbf{I}_{\frac{N^2}{4}}$ ,

$$\sum_{j=0}^{N_c-1} (\mathbf{B}^{(j)})^* \mathbf{B}^{(j)} = \frac{N^2}{4} \sum_{j=0}^{N_c-1} \text{diag}(\text{vec}(\overline{\tilde{\mathbf{s}}^{(j)}})) (\mathbf{E}_4 \otimes \mathbf{I}_{\frac{N^2}{4}}) \text{diag}(\text{vec}(\tilde{\mathbf{s}}^{(j)}))$$

is a block diagonal matrix with only 4 entries per row and per column. The right-hand-side of (3.11) is given by

$$\begin{aligned} \sum_{j=0}^{N_c-1} (\mathbf{B}^{(j)})^* \text{diag}(\text{vec}(\mathcal{P}_1)) \text{vec}(\mathbf{y}^{(j)}) &= \sum_{j=0}^{N_c-1} \text{diag}(\text{vec}(\overline{\tilde{\mathbf{s}}^{(j)}})) (\mathbf{F}_N^* \otimes \mathbf{F}_N^*) (\mathbf{P}_1 \otimes \mathbf{I}_N) \text{vec}(\mathbf{y}^{(j)}) \\ &= N^2 \sum_{j=0}^{N_c-1} \text{vec}(\overline{\tilde{\mathbf{s}}^{(j)}}) \circ \text{vec}(\mathbf{F}_N^{-1}(\mathbf{y}^{(j)} \mathbf{P}_1) \mathbf{F}_N^{-1}) = N^2 \sum_{j=0}^{N_c-1} \text{vec}(\overline{\tilde{\mathbf{s}}^{(j)}}) \circ \text{vec}(\check{\mathbf{y}}_{\mathbf{P}_1}^{(j)}), \end{aligned}$$

where  $\check{\mathbf{y}}_{\mathbf{P}_1}^{(j)} = (\check{y}_{\mathbf{P}_1, (k,\ell)}^{(j)})_{(k,\ell) \in \Lambda_N}$  denotes the inverse 2D FFT of the incomplete  $k$ -space data  $\mathcal{P}_1 \circ \mathbf{y}^{(j)}$ . The structure of  $\sum_{j=0}^{N_c-1} (\mathbf{B}^{(j)})^* \mathbf{B}^{(j)}$  implies that the large system

(3.11) falls apart into  $\frac{N^2}{4}$  small systems of size  $4 \times 4$ . For  $k = -\frac{N}{2}, \dots, \frac{N}{2} - 1$  and  $\ell = -\frac{N}{8}, \dots, \frac{N}{8} - 1$ , we have to solve

$$\frac{1}{4} \left( \frac{4}{N^2} \beta \mathbf{I}_4 + \sum_{j=0}^{N_c-1} \bar{\mathbf{s}}_{k,\ell}^{(j)} (\mathbf{s}_{k,\ell}^{(j)})^T \right) \begin{pmatrix} m_{k,\ell-\frac{3N}{8}} \\ m_{k,\ell-\frac{N}{8}} \\ m_{k,\ell+\frac{N}{8}} \\ m_{k,\ell+\frac{3N}{8}} \end{pmatrix} = \left( \sum_{j=0}^{N_c-1} \bar{\mathbf{s}}_{k,\ell}^{(j)} \circ \begin{pmatrix} \check{y}_{\mathbf{P}_1,k,\ell-\frac{3N}{8}}^{(j)} \\ \check{y}_{\mathbf{P}_1,k,\ell-\frac{N}{8}}^{(j)} \\ \check{y}_{\mathbf{P}_1,k,\ell+\frac{N}{8}}^{(j)} \\ \check{y}_{\mathbf{P}_1,k,\ell+\frac{3N}{8}}^{(j)} \end{pmatrix} \right),$$

with  $\mathbf{s}_{k,\ell}^{(j)} = (s_{k,\ell-\frac{3N}{8}}^{(j)}, s_{k,\ell-\frac{N}{8}}^{(j)}, s_{k,\ell+\frac{N}{8}}^{(j)}, s_{k,\ell+\frac{3N}{8}}^{(j)})^T \in \mathbb{C}^4$  to recover  $\mathbf{m}$ . These equation systems are implemented in Algorithm 3.6. For other patterns one can similarly find a decomposition of  $\sum_{j=0}^{N_c-1} (\mathbf{B}^{(j)})^* \mathbf{B}^{(j)}$ .

Finally, we employ the obtained insights on the structure of the matrix  $\sum_{j=0}^{N_c-1} (\mathbf{B}^{(j)})^* \mathbf{B}^{(j)}$  in (3.11) (with  $\beta = 0$ ) to find simple conditions for invertibility of this matrix, such that the regularization with  $\beta > 0$  is not needed. First, we give an invertibility condition in terms of the vectors  $\mathbf{c}^{(j)}$  obtained in the steps 1-3 of the MOCCA Algorithm 3.2.

**Theorem 4.5** *Let  $\mathbf{c}^{(j)} = (c_{\mathbf{r}}^{(j)})_{\mathbf{r} \in \Lambda_L} \in \mathbb{C}^{L^2}$ ,  $j = 0, \dots, N_c - 1$ , be the vectors determining the (vectorized) coil sensitivities  $\text{vec}(\mathbf{s}^{(j)}) = \mathbf{W}\mathbf{c}^{(j)}$  in (2.3) and let  $(c_{\mathbf{n}}^{(j)})_{\mathbf{n} \in \Lambda_N} \in \mathbb{C}^{N^2}$  be the extensions of  $\mathbf{c}^{(j)}$  to  $\Lambda_N$  with  $c_{\mathbf{n}}^{(j)} = 0$  for  $\mathbf{n} \in \Lambda_N \setminus \Lambda_L$ . Further, let  $\sum_{j=0}^{N_c-1} |s_{\nu}^{(j)}|^2 > 0$  for all  $\nu \in \Lambda_N$ . Then  $\sum_{j=0}^{N_c-1} (\mathbf{B}^{(j)})^* \mathbf{B}^{(j)}$  is invertible if and only if the sparse matrix*

$$\begin{pmatrix} (\hat{s}_{(\nu-\mathbf{n}) \bmod \Lambda_N}^{(0)})_{\nu \in \Lambda_{\mathcal{P}}, \mathbf{n} \in \Lambda_N} \\ (\hat{s}_{(\nu-\mathbf{n}) \bmod \Lambda_N}^{(1)})_{\nu \in \Lambda_{\mathcal{P}}, \mathbf{n} \in \Lambda_N} \\ \vdots \\ (\hat{s}_{(\nu-\mathbf{n}) \bmod \Lambda_N}^{(N_c-1)})_{\nu \in \Lambda_{\mathcal{P}}, \mathbf{n} \in \Lambda_N} \end{pmatrix} := N^2 \begin{pmatrix} (c_{(\nu-\mathbf{n}) \bmod \Lambda_N}^{(0)})_{\nu \in \Lambda_{\mathcal{P}}, \mathbf{n} \in \Lambda_N} \\ (c_{(\nu-\mathbf{n}) \bmod \Lambda_N}^{(1)})_{\nu \in \Lambda_{\mathcal{P}}, \mathbf{n} \in \Lambda_N} \\ \vdots \\ (c_{(\nu-\mathbf{n}) \bmod \Lambda_N}^{(N_c-1)})_{\nu \in \Lambda_{\mathcal{P}}, \mathbf{n} \in \Lambda_N} \end{pmatrix} \in \mathbb{C}^{N_c |\Lambda_{\mathcal{P}}| \times N^2} \quad (4.9)$$

has rank  $N^2$ . In particular, if  $\sum_{j=0}^{N_c-1} (\mathbf{B}^{(j)})^* \mathbf{B}^{(j)}$  is invertible, then  $N_c |\Lambda_{\mathcal{P}}| \geq N^2$  and  $\Lambda_N \subset (\nu + \Lambda_L)_{\nu \in \Lambda_{\mathcal{P}}}$ .

**Proof:** Let  $\mathbf{g} \in \mathbb{C}^{N^2}$  be a vector with  $\mathbf{g}^* (\sum_{j=0}^{N_c-1} (\mathbf{B}^{(j)})^* \mathbf{B}^{(j)}) \mathbf{g} = 0$ . Since  $(\mathbf{B}^{(j)})^* \mathbf{B}^{(j)}$  is positive semidefinite for all  $j = 0, \dots, N_c - 1$ , it follows that

$$\mathbf{g}^* (\mathbf{B}^{(j)})^* \mathbf{B}^{(j)} \mathbf{g} = \|\mathbf{B}^{(j)} \mathbf{g}\|_2^2 = 0, \quad j = 0, \dots, N_c - 1,$$

i.e.,  $\mathbf{B}^{(j)} \mathbf{g} = \mathbf{0}$  for  $j = 0, \dots, N_c - 1$ . By definition, we have  $\mathbf{B}^{(j)} = \mathcal{P}\mathcal{F}\text{diag}(\text{vec}(\hat{\mathbf{s}}^{(j)})) = \mathcal{P}\mathcal{F}\text{diag}(\text{vec}((\mathbf{d}^+)^{\frac{1}{2}} \circ \mathbf{s}^{(j)}))$  and defining  $\tilde{\mathbf{g}} := \text{vec}((\mathbf{d}^+)^{\frac{1}{2}}) \circ \mathbf{g} = \text{diag}(\text{vec}((\mathbf{d}^+)^{\frac{1}{2}})) \mathbf{g}$  with  $\mathbf{d}^+$  as in step 4 of Algorithm 3.2 we find

$$\mathbf{B}^{(j)} \mathbf{g} = \mathcal{P}\mathcal{F}(\text{diag}(\text{vec}(\mathbf{s}^{(j)} \circ (\mathbf{d}^+)^{\frac{1}{2}})) \mathbf{g}) = \mathcal{P}\mathcal{F} \text{vec}(\mathbf{s}^{(j)}) \circ \tilde{\mathbf{g}} = \frac{1}{N^2} \mathcal{P}((\mathcal{F} \text{vec}(\mathbf{s}^{(j)})) * (\mathcal{F} \tilde{\mathbf{g}})) = \mathbf{0},$$

where  $*$  denotes the 2D discrete  $N$ -periodic convolution. From  $\text{vec}(\mathbf{s}^{(j)}) = \mathbf{W}\mathbf{c}^{(j)}$  we obtain  $\text{vec}(\hat{\mathbf{s}}^{(j)}) := \mathcal{F} \text{vec}(\mathbf{s}^{(j)}) = N^2 (c_{\nu}^{(j)})_{\nu \in \Lambda_N}$  is the zero-extension of  $\mathbf{c}^{(j)}$  from  $\Lambda_L$  to

$\Lambda_N$ . Hence,

$$\begin{aligned} \mathcal{P}(\mathcal{F}\text{vec}(\mathbf{s}^{(j)}) * \mathcal{F}\tilde{\mathbf{g}}) &= (\hat{s}_{(\boldsymbol{\nu}-\mathbf{r})\bmod\Lambda_N}^{(j)})_{\boldsymbol{\nu}\in\Lambda_{\mathcal{P}},\mathbf{r}\in\Lambda_N}(\mathcal{F}\tilde{\mathbf{g}}) \\ &= N^2(c_{(\boldsymbol{\nu}-\mathbf{r})\bmod\Lambda_N}^{(j)})_{\boldsymbol{\nu}\in\Lambda_{\mathcal{P}},\mathbf{r}\in\Lambda_N}(\mathcal{F}\tilde{\mathbf{g}}) = \mathbf{0} \end{aligned}$$

for  $j = 0, \dots, N_c - 1$ . Thus,  $\tilde{\mathbf{g}} = \mathbf{0}$ , if and only if the matrix in (4.9) has full rank  $N^2$ . Therefore, also  $\mathbf{g} = \mathbf{0}$ , since  $\mathbf{d}^+$  has only positive components. In particular, the invertibility of  $\sum_{j=0}^{N_c-1} (\mathbf{B}^{(j)})^* \mathbf{B}^{(j)}$  implies  $N_c |\Lambda_{\mathcal{P}}| \geq N^2$  and  $\Lambda_N \subset (\boldsymbol{\nu} + \Lambda_L)_{\boldsymbol{\nu}\in\Lambda_{\mathcal{P}}}$ . ■

Similarly, we obtain a condition for other regular patterns of acquired data, as e.g. for the special example that each second row and each second column of the  $k$ -space data is acquired.

**Corollary 4.1** *Assume that the index set of acquired measurements  $\Lambda_{\mathcal{P}}$  contains beside the ACS region index set  $\Lambda_{M+L-1}$  the set  $2\Lambda_{N/2}$ , i.e., every second index in  $x$ -direction and  $y$ -direction. Then, the matrix  $\sum_{j=0}^{N_c-1} (\mathbf{B}^{(j)})^* \mathbf{B}^{(j)}$  is invertible, if the  $(N_c \times 4)$ -matrices*

$$\mathbf{G}_{\mathbf{n}} := \begin{pmatrix} s_{\mathbf{n}+(\frac{N}{4},\frac{N}{4})}^{(0)} & s_{\mathbf{n}+(\frac{N}{4},-\frac{N}{4})}^{(0)} & s_{\mathbf{n}+(-\frac{N}{4},\frac{N}{4})}^{(0)} & s_{\mathbf{n}+(-\frac{N}{4},-\frac{N}{4})}^{(0)} \\ s_{\mathbf{n}+(\frac{N}{4},\frac{N}{4})}^{(1)} & s_{\mathbf{n}+(\frac{N}{4},-\frac{N}{4})}^{(1)} & s_{\mathbf{n}+(-\frac{N}{4},\frac{N}{4})}^{(1)} & s_{\mathbf{n}+(-\frac{N}{4},-\frac{N}{4})}^{(1)} \\ \vdots & \vdots & \vdots & \vdots \\ s_{\mathbf{n}+(\frac{N}{4},\frac{N}{4})}^{(N_c-1)} & s_{\mathbf{n}+(\frac{N}{4},-\frac{N}{4})}^{(N_c-1)} & s_{\mathbf{n}+(-\frac{N}{4},\frac{N}{4})}^{(N_c-1)} & s_{\mathbf{n}+(-\frac{N}{4},-\frac{N}{4})}^{(N_c-1)} \end{pmatrix} \quad (4.10)$$

have full rank 4 for each  $\mathbf{n} \in \Lambda_{\frac{N}{2}}$ .

**Proof:** The proof follows directly from the observations in this section and in Section 3.3.2, Remark 3.3, where the matrices  $\mathbf{G}_{\mathbf{n}} = \mathbf{G}_{(k,\ell)}$  with  $k, \ell = -\frac{N}{4}, \dots, \frac{N}{4} - 1$  need to be invertible to recover the components of  $\mathbf{m}$ . ■

## 5 Numerical Results

In this section we test the Algorithms 3.2-3.6 with parallel MRI data from two different brain images. The data sets `brain_8ch` and `brain_32ch` (using only 8 coils) are in the `ESPIRiT` toolbox and have been also used to in [42]. The magnitudes of the coil images  $|\mathcal{F}^{-1}\mathbf{y}^{(j)}|$  for these data sets are illustrated in Figure 2.

The 8 coil images in the first data set are of size  $200 \times 200$ , i.e.,  $N = 200$ . From the second data set we have taken 8 coils of size  $192 \times 192$ . We compare the reconstruction results of our MOCCA algorithm with the results of GRAPPA, SPIRiT, ESPIRiT, L1-ESPIRiT and JSENSE using the peak-signal-to-noise ratio (PSNR) and the structural similarity index measure (SSIM) (using the internal functions in Matlab), where the `sos` reconstruction from complete  $k$ -space data is taken as the ground truth.

The performance of the MOCCA algorithm depends on the chosen support  $\Lambda_L$  of the trigonometric polynomials determining the coil sensitivities. If we take the iterative Algorithm 3.4 to solve the least squares problem, we can profit from using a suitable number of iteration steps. Further, the results of the MOCCA Algorithm 3.2 can be improved by employing the smoothing procedure proposed in Section 3.4. The size of the calibration area is always taken similarly as for the other algorithms.

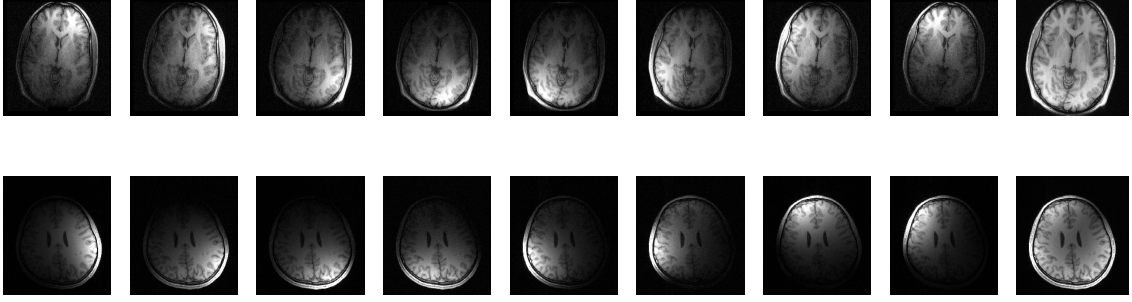


**Figure 2:** Magnitudes of the coil images for the two used test data sets together with the full sos reconstruction at the end.

We start with reconstructions from  $k$ -space data of the first data set, where outside of the ACS region the following scheme for acquired incomplete data with reduction rate  $R$  is taken:

every second column,  $R = 2$ ,  $(1, 1/2)$ ,

every third column,  $R = 3$ ,  $(1, 1/3)$ ,

every fourth column,  $R = 4$ ,  $(1, 1/4)$ ,

every second row and every second column,  $R = 4$ ,  $(1/2, 1/2)$ ,

every second row and every third column,  $R = 6$ ,  $(1/2, 1/3)$ .

The results are summarized in Table 1.

For MOCCA we have used  $\beta = 0.001$  and a fixed number of iterations in Algorithm 3.4. Further, the support  $\Lambda_L$  of the coil sensitivities in  $k$ -space is given by  $\Lambda_5 = \{-2, -1, 0, 1, 2\} \times \{-2, -1, 0, 1, 2\}$ , i.e.,  $L^2 = 25$  parameters are used per coil sensitivity. In Figure 5(left), we display the singular values of the MOCCA-matrix  $\mathbf{A}_M$  in (3.10) obtained for the first data set with  $L = 5$ . The decay of the singular values of  $\mathbf{A}_M$  shows that, corresponding to the theoretical observations in Sections 3 and 4, the smallest singular value of  $\mathbf{A}_M$  is close to 0. For this first data set and  $L = 5$ , the singular vector corresponding to the smallest singular value can be directly taken to reconstruct the coil sensitivities. In our results given in Table 1, we have used a linear combination of two singular vectors  $\mathbf{c} = \mathbf{c}_1 + \alpha \mathbf{c}_2$  in order to improve the reconstruction result, where  $\mathbf{c}_1$  corresponds to the smallest singular value 0.1537 and  $\mathbf{c}_2$  to the second smallest value 0.1803. For  $R = 2, 3, 4$  we have employed  $\alpha = 0.2$  and for  $R = 6$ , we used  $\alpha = i$ .

In Table 1 we present the results for MOCCA and MOCCA-S (MOCCA with a smoothing step as in Section 3.4) obtained by Algorithm 3.6 and by the iterative Algorithm 3.4, where the employed number of iterations depends on  $R$  and is indicated in Table 1 with the numbers in brackets. For example, for  $R = 2$ , we used 12 iterations. For the smoothing step, we used  $\lambda = 0.00045$  for  $R = 2$ ,  $\lambda = 0.0018$  for  $R = 3$  and  $R = 4(1, \frac{1}{4})$ ,  $\lambda = 0.0015$  for  $R = 4(\frac{1}{2}, \frac{1}{2})$ , and  $\lambda = 0.0035$  for  $R = 6$ . Interestingly, the recovery results for the direct fast MOCCA Algorithm 3.6 outperform the iterative MOCCA Algorithm 3.4 for the cases  $R = 2$ ,  $R = 3$ , and works equally well for  $R = 4(\frac{1}{2}, \frac{1}{2})$ , while being much worse for the other cases. We argue that, since the direct algorithm solves small independent linear systems, and does not directly exploit the full data knowledge in the ACS region, local model inconsistencies in the data directly lead to larger local solution errors for higher reduction factors. Note that the performance of MOCCA further improves for larger  $k$ -space support of sensitivities, i.e.,  $L > 7$ .

For GRAPPA and SPIRiT we applied the implementation `demo_11_spirit_pocs.m`

in the ESPIRiT Matlab toolbox with parameters given there for this data set, i.e., SPIRiT kernel size  $kSize = [5, 5]$ ,  $nIter = 20$  iterations, Tykhonov regularization parameter  $CalibTyk = 0.01$  in the calibration, and  $wavWeight = 0.0015$  for wavelet soft-thresholding regularization in the reconstruction. For ESPIRiT, we have taken `demo_ESPIRiT_recon.m` from the ESPIRiT toolbox with  $ncalib = 24$  ( $24 \times 24$  calibration area), kernel window size  $ksize = [6, 6]$ ,  $eigThresh_k = 0.02$ ,  $eigThresh_im = 0.9$ , and two sets of eigenmaps. For L1-ESPIRiT, we used `demo_ESPIRiT_L1_recon.m` from the ESPIRiT toolbox, which had been created for this data set with the ESPIRiT parameters as above and the setting for the L1-reconstruction with  $nIterCG = 5$  CG iterations for the PI part,  $nIterSplit = 15$  splitting iterations for CS part,  $splitWeight = 0.4$ , and  $lambda = 0.0025$  for  $R = 2$  and optimized parameters  $splitWeight = 0.2$ ,  $lambda = 0.7$  for  $R > 2$ . For JSENSE we used the software by the authors of [45] and tried to adapt the number of iterations for alternating minimization as well as the polynomial degree to approximate the sensitivities for optimal reconstruction results in Table 1. The original implementation only works, if the image dimension is a multiple of the considered reduction rate, and if the data in only one direction are non-acquired. For  $R = 3$  we have therefore adapted the number of columns on the coil data  $\mathbf{y}^{(j)}$  from 200 to 198. Unfortunately, due to the required alternating minimization steps, JSENSE is more time consuming than the other algorithms.

**Table 1:** Comparison of the reconstruction performance for the incomplete data from the first data set.

method	measure	$R = 2, (1, \frac{1}{2})$	$R = 3, (1, \frac{1}{3})$	$R = 4, (1, \frac{1}{4})$	$R = 4, (\frac{1}{2}, \frac{1}{2})$	$R = 6, (\frac{1}{2}, \frac{1}{3})$
GRAPPA	PSNR	41.4367	36.2093	30.3212	34.8741	28.9493
	SSIM	0.9638	0.9039	0.7561	0.8821	0.7236
SPIRiT	PSNR	26.7296	28.3496	26.7414	30.8745	29.6801
	SSIM	0.9441	0.8794	0.7192	0.8871	0.7307
ESPIRiT	PSNR	37.2218	35.1977	32.0629	35.4497	32.6245
	SSIM	0.8138	0.7808	0.7022	0.7848	0.7164
L1-ESPIRiT	PSNR	37.3810	35.9555	<b>34.1941</b>	35.9088	33.5887
	SSIM	0.8279	0.7689	0.7612	0.7714	0.7589
JSENSE	PSNR	33.5558	34.0555	30.8670		
	SSIM	0.8723	0.8665	0.7818		
MOCCA (L=5)	PSNR	(12)38.7136	(40)35.1875	(75)32.0755	(50)35.6563	(90)32.0203
	SSIM	0.9119	0.8795	0.8111	0.8896	0.7995
MOCCA-S (L=5)	PSNR	(12)39.4055	(40)36.7334	(75)33.2165	(50) <b>37.2826</b>	(90) <b>33.6516</b>
	SSIM	0.9241	0.9301	<b>0.8845</b>	<b>0.9354</b>	<b>0.8897</b>
MOCCA direct (L=5)	PSNR	41.3746	35.1676	29.1279	35.0675	27.8404
	SSIM	0.9643	0.8859	0.6491	0.8815	0.6078
MOCCA-S direct (L=5)	PSNR	<b>42.1886</b>	<b>37.4517</b>	32.2398	36.7925	29.3610
	SSIM	<b>0.9717</b>	<b>0.9369</b>	0.7876	0.9294	0.7119

In Figure 3, we exemplarily represent the reconstruction results for the reduction factor  $R = 3$  (every third column acquired) and the corresponding error maps. Further, in Figure 4, we illustrate the magnitude and the phase of the 8 normalized coil sensitivities  $\tilde{\mathbf{s}}^{(j)}$  obtained for the first data set. Before pointwise multiplication with  $\text{sign}(m_{\mathbf{n}})$ , the sensitivities have smooth magnitude and phase, since they are samples of pointwisely normalized trigonometric polynomials of small degree, i.e., samples of trigonometric rational functions.

For the second data set, we want to illustrate that the chosen support size of the trigonometric polynomials to evaluate the coil sensitivities plays an important role for obtaining very good reconstruction results. We compare with GRAPPA, ESPIRiT with

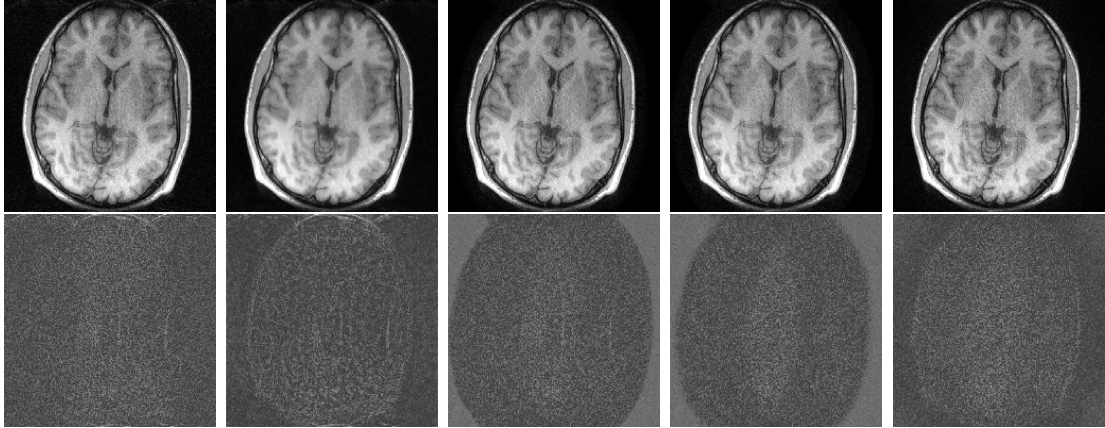


**Figure 3:** Reconstruction results for the first data set obtained from a third of the  $k$ -space data of 8 coils (every third column acquired) for different methods. From left to right: (1) MOCCA using Algorithm 3.2 (taking Algorithm 3.4 with 40 iterations), (2) MOCCA-S (with 40 iterations and smoothing), (3) L1-ESPIRiT, (4) ESPIRiT and (5) GRAPPA. Corresponding error maps are given below. All error images use the same scale with relative error in  $[0, 0.12]$ , where 0 corresponds to black and 0.12 to white.

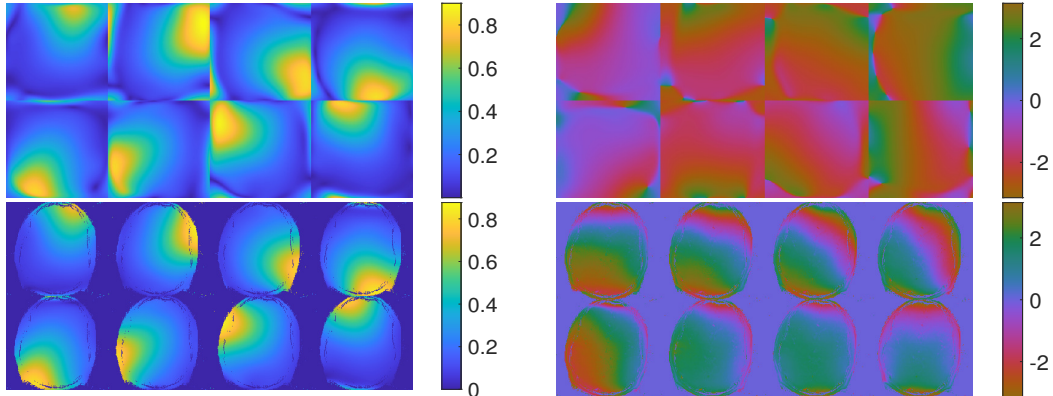


**Figure 4:** Magnitude (left) and phase (in  $[-\pi, \pi]$ ) (right) of the 8 coil sensitivities obtained for MRI reconstruction for  $L = 5$  for the first data set before and after multiplication with  $\text{sign}(\mathbf{m})$ , see step 7 of Algorithm 3.2. The normalized sensitivities are samples of bivariate trigonometric polynomials with  $L^2 = 25$  nonzero coefficients, pointwisely multiplied with the normalization factors  $(\mathbf{d}^+)^{\frac{1}{2}}$  to ensure the sos condition.

parameters fixed as for the first data set, for L1-ESPIRiT with optimized parameters  $\text{splitWeight} = 0.1$ ,  $\text{lambda} = 0.0002$ , and also show the results of MOCCA for different support sizes in Table 2. For MOCCA, the numbers in brackets give the numbers of iterations in Algorithm 3.4. As before, MOCCA-S employs the smoothing procedure in Section 3.4 as a post-processing step, where the parameter  $\lambda$  is taken in dependence of  $R$ . We used  $\lambda = 0.00015$  for  $R = 2$ ,  $\lambda = 0.0005$  for  $R = 3$  and  $R = 4(\frac{1}{2}, \frac{1}{2})$ ,  $\lambda = 0.0013$  for  $R = 4(1, \frac{1}{4})$  and  $R = 6$ . The results MOCCA direct and MOCCA-S direct are obtained by Algorithm 3.6. As before, Algorithm 3.6 outperforms Algorithm 3.4 for  $R = 2, 3$ , and  $R = 4(\frac{1}{2}, \frac{1}{2})$  and is worse for the other cases.

Since the parallel MRI data do not exactly fit our model with the chosen support sizes, the MOCCA matrix  $\mathbf{A}_M$  obtained from the second data set possesses several

very small singular values, see Figure 5. While for the first data set with  $L = 5$  and  $M = 20$  (i.e., ACS area of size  $24 \times 24$ ), the matrix  $\mathbf{A}_M$  contains only two singular values being smaller than  $\frac{\sigma_1}{100}$  (where  $\sigma_1$  denotes the largest singular value), we observe for the second data set (with  $M = 20$  and  $L = 5$ ) that already 11 values are below this bound. For support size  $L = 7$  we have 45 values smaller than  $\frac{\sigma_1}{100}$ , and for  $L = 9$ , even 139 values.

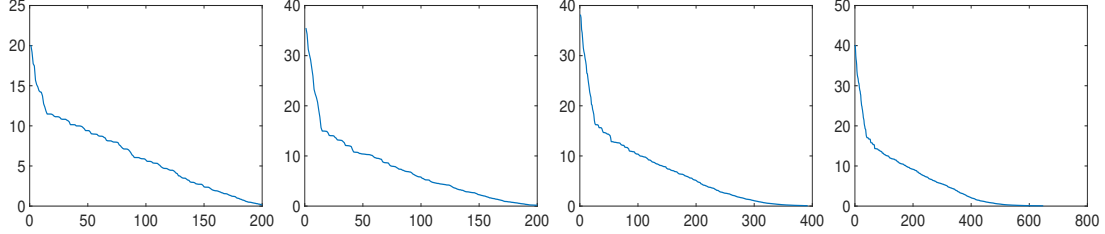


**Figure 5:** Illustration of the singular values of the matrix  $\mathbf{A}_M$  for the first and the second data set. From left to right: (1) Singular values of  $\mathbf{A}_M$  with  $L = 5$  and  $25 \cdot 8 = 200$  columns for the first data set. (2) Singular values of  $\mathbf{A}_M$  with  $L = 5$  and  $25 \cdot 8 = 200$  columns, (3) with  $L = 7$  and  $49 \cdot 8 = 392$  columns, and (4) with  $L = 9$  and  $81 \cdot 8 = 648$  columns for the second data set.

Therefore, to compute the coefficient vector  $\mathbf{c}$  (see step 2 of Algorithm 3.2), we propose to take a suitable linear combination of several singular vectors corresponding to the smallest singular values of  $\mathbf{A}_M$ . More exactly, for reconstruction from the second data set, we employ a linear combination of the form

$$\mathbf{c} = \sum_{\nu=1}^{N_s} \alpha_\nu \mathbf{c}_\nu \quad (5.1)$$

with  $N_s \geq 1$ ,  $\alpha_\nu \in \mathbb{C}$  and with  $\mathbf{c}_\nu$  being a singular vector of  $\mathbf{A}_M$  corresponding to its  $\nu$ -th smallest singular value. Our numerical experiments have shown that this linear combination should be taken such that the final vector  $\mathbf{c} = (\mathbf{c}^{(j)})_{j=0}^{N_c-1}$  leads via step 3 of Algorithm 3.2 to sensitivities  $\mathbf{s}^{(j)}$ , where the matrix  $\mathbf{d} = (d_{\mathbf{n}})_{\mathbf{n} \in \Lambda_N} = \sum_{j=0}^{N_c-1} \bar{\mathbf{s}}^{(j)} \circ \mathbf{s}^{(j)}$  does not have very small entries. In other words, one should exploit the freedom to choose  $\mathbf{c} = (\mathbf{c}^{(j)})_{j=0}^{N_c-1}$  in (5.1) to achieve sensitivities  $\mathbf{s}^{(j)}$ , which are already close to satisfying the sos condition, such that all components  $d_{\mathbf{n}}$ ,  $\mathbf{n} \in \Lambda_N$  are of similar size.

We have implemented the following method to compute  $\boldsymbol{\alpha} = (\alpha_\nu)_{\nu=1}^{N_s}$  determining  $\mathbf{c}$  in (5.1). Let  $\mathbf{A}_M = \mathbf{U}\boldsymbol{\Sigma}\mathbf{V}$  denote the SVD of the MOCCA-matrix  $\mathbf{A}_M$  in (3.10), which is computed in step 2 of Algorithm 3.2. Further, let  $\mathbf{V}_{L^2 N_c, N_s}$  be the partial matrix of  $\mathbf{V}$  containing the last  $N_s$  eigenvectors of  $\mathbf{A}_M$  and  $\mathbf{w} := (\mathbf{e}_0^T, \mathbf{e}_0^T, \dots, \mathbf{e}_0^T)^T \in \mathbb{C}^{L^2 N_c}$ , with  $\mathbf{e}_0 = (\delta_{0,k})_{k=-(L^2-1)/2}^{(L^2-1)/2}$  and the Kronecker symbol  $\delta_{0,k} := 0$  for  $k \neq 0$  and  $\delta_{0,0} := 1$ . Then we take  $\boldsymbol{\alpha} = \mathbf{V}_{L^2 N_c, N_s}^* \mathbf{w}$ . The question of how to take  $N_s$  suitably and the problem of finding better methods to choose  $\alpha_\nu$  is still open und requires further investigations.

In Table 2 we have used this approach for  $L = 5$  with  $N_s = 15$  for  $R = 4$ ,  $(\frac{1}{2}, \frac{1}{2})$ ,  $R = 6$ , and  $N_s = 30$  otherwise, for  $L = 7$  with  $N_s = 47$ , and for  $L = 9$  with  $N_s = 45$  to achieve the presented results. We observe very high SSIM values for the MOCCA algorithm, which are particularly much higher than for ESPIRiT. This may be due to the fact that the errors occurring for the MOCCA reconstructions are very small also outside the boundary of the brain.

**Table 2:** Comparison of the reconstruction performance for the incomplete data from the second data set.

method	measure	$R = 2, (1, \frac{1}{2})$	$R = 3, (1, \frac{1}{3})$	$R = 4, (1, \frac{1}{4})$	$R = 4, (\frac{1}{2}, \frac{1}{2})$	$R = 6, (\frac{1}{2}, \frac{1}{3})$
GRAPPA	PSNR	47.2028	42.9704	37.6036	41.5961	38.5314
	SSIM	0.9796	0.9573	0.9167	0.9498	0.9244
ESPIRiT	PSNR	40.3668	39.7082	37.1418	39.6082	38.4716
	SSIM	0.7490	0.7462	0.7243	0.7461	0.7354
L1-ESPIRiT	PSNR	40.2750	39.7584	38.1926	39.6515	38.8431
	SSIM	0.7465	0.7520	0.7455	0.7521	0.7503
MOCCA (L=5)	PSNR	(10)42.6611	(50)40.3835	(70)34.8179	(50)40.6865	(90)35.9914
	SSIM	0.9258	0.9474	0.8769	0.9472	0.8752
MOCCA-S (L=5)	PSNR	(10)43.2025	(50)41.7574	(70)35.8326	(50)42.2273	(90)37.5114
	SSIM	0.9314	0.9675	0.9192	0.9679	0.9239
MOCCA (L=7)	PSNR	(10)43.5172	(50)41.9112	(70)37.3703	(50)41.7795	(90)37.4211
	SSIM	0.9251	0.9461	0.9143	0.9534	0.9011
MOCCA-S (L=7)	PSNR	(10)44.0399	(50)43.5151	(70)38.9200	(50)43.5679	(90)39.3194
	SSIM	0.9299	0.9630	0.9537	0.9729	0.9463
MOCCA (L=9)	PSNR	(10)43.2813	(50)41.7241	(70)38.0292	(50)41.2087	(90)37.9957
	SSIM	0.9199	0.9437	0.9214	0.9489	0.9127
MOCCA-S (L=9)	PSNR	(10)43.7645	(50)43.1347	(70) <b>39.7013</b>	(50)42.6955	(90) <b>40.0862</b>
	SSIM	0.9245	0.9597	<b>0.9579</b>	0.9675	<b>0.9571</b>
MOCCA direct (L=7)	PSNR	47.4233	42.2531	35.8053	42.1402	34.4736
	SSIM	0.9844	0.9615	0.8838	0.9616	0.8293
MOCCA-S direct (L=7)	PSNR	<b>47.9400</b>	<b>43.8822</b>	38.0142	<b>43.9457</b>	36.4445
	SSIM	<b>0.9866</b>	<b>0.9764</b>	0.9374	<b>0.9792</b>	0.8954

In Figure 6, we exemplarily represent the reconstruction results for  $R = 4$  (every fourth column acquired) and the corresponding error maps for the second data set. The MOCCA-S reconstructions for  $L = 9$  and  $L = 11$  in Figure 6 do not contain obviously visible aliasing artifacts. The GRAPPA and ESPIRiT reconstructions in Figure 6 contain slightly visible aliasing artifacts. Note that a high PSNR value not always implies a very good visual reconstruction result since pointwise large errors are not strongly punished by this measure.

Finally, in Figure 7, we illustrate the magnitude and the phase of the 8 normalized coil sensitivities  $\tilde{\mathbf{s}}^{(j)}$  obtained for the second data set with  $L = 9$ . Since these sensitivities are constructed from bivariate trigonometric polynomials of higher degree (with 81 nonzero coefficients) they possess a more oscillatory behavior in magnitude and phase than the sensitivities for the first data set for  $L = 5$ .

The implementation of the MOCCA algorithms have been performed in Matlab. The presentation of coils in Figures 4 and 7 uses `imshow3.m` by M. Lustig and `phasemap.m` by C. Greene. The code is available at <https://na.math.uni-goettingen.de>.

## 6 Conclusions

Previous sub-space methods in parallel MRI [38, 42, 10, 23] are usually based on the assumption that the block Hankel matrix  $(\mathbf{Y}_{N,L}^{(0)}, \mathbf{Y}_{N,L}^{(1)}, \dots, \mathbf{Y}_{N,L}^{(N_c-1)}) \in \mathbb{C}^{N^2 \times L^2 N_c}$ , where  $\mathbf{Y}_{N,L}^{(j)} = (y_{(\nu-r) \bmod \Lambda_N}^{(j)})_{\nu \in \Lambda_N, r \in \Lambda_L}$  with  $L$  being a suitable small window size, has low rank. More exactly, it is assumed that the rank of this matrix is essentially smaller than  $L^2 N_c$ . The application of these methods based on (structured) low-rank matrix approximations and the study the reconstructed sensitivities  $\mathbf{s}^{(j)}$  leads to the

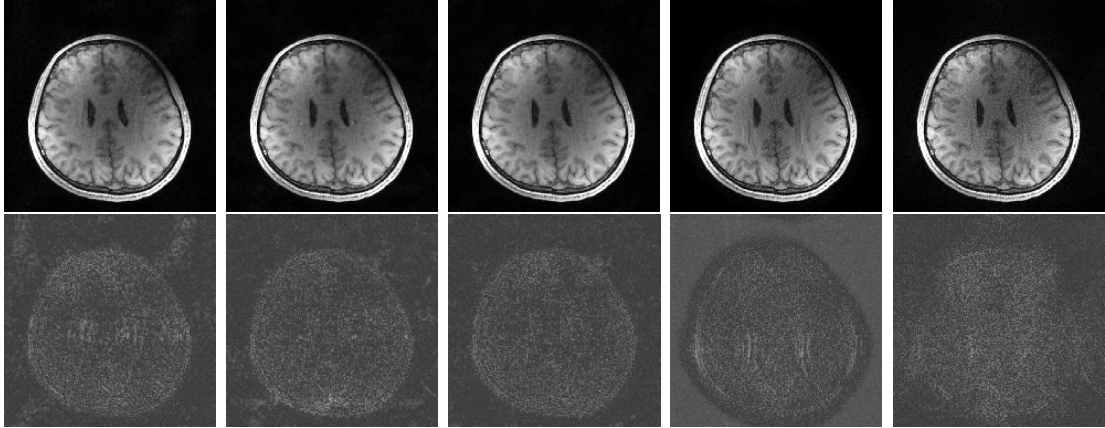


**Figure 6:** Reconstruction results obtained from a fourth of the  $k$ -space data of the second data set with 8 coils (every fourth column acquired) for MOCCA-S, ESPIRiT, and GRAPPA. From left to right: (1) MOCCA-S with  $L = 7$ , (2) MOCCA-S with  $L = 9$ , and (3) MOCCA-S with  $L = 11$ , all using Algorithm 3.2 with Algorithm 3.4 and smoothing with  $\lambda = 0.002$ , (4) ESPIRiT, (5) GRAPPA. Corresponding error maps are given below, where darker means smaller error. All error images use the same scale with relative error in  $[0, 0.14]$ , where 0 corresponds to black and 0.14 to white.

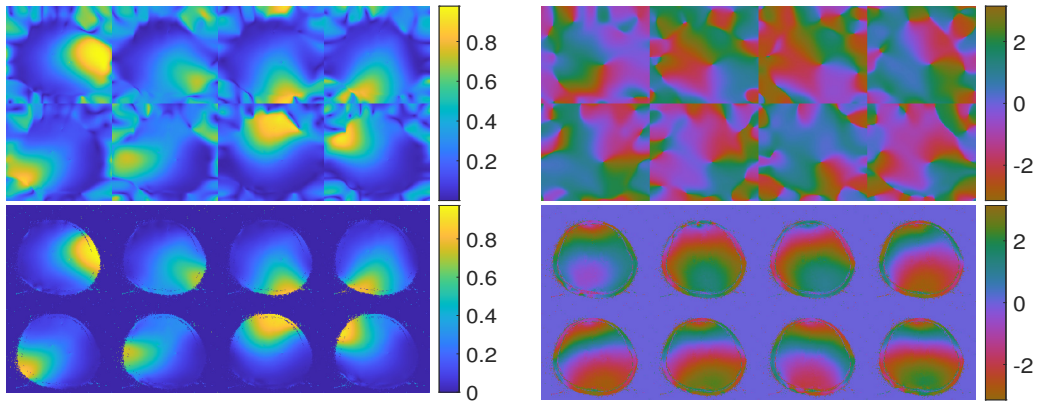


**Figure 7:** Magnitude (left) and phase (in  $[-\pi, \pi]$ ) (right) of the 8 coil sensitivities obtained for MRI reconstruction for  $L = 9$  for the second data set before and after multiplication with  $\text{sign}(\mathbf{m})$ , see step 7 of Algorithm 3.2. The normalized sensitivities are samples of bivariate trigonometric polynomials with  $L^2 = 81$  nonzero coefficients, pointwisely multiplied with the normalization factors  $(\mathbf{d}^+)^{\frac{1}{2}}$  to ensure the sos condition.

observation that the  $\mathbf{s}^{(j)}$  usually have (approximately) a small support in  $k$ -space, see e.g. [38, 42]. Our new MOCCA approach directly computes the sensitivities and the magnetization image based on the a priori fixed model (2.2) (resp. (2.4)) and can therefore be seen as a counterpart of the known algorithms. Our different view provides several advantages: We can provide simple and fast reconstruction algorithms for incomplete  $k$ -space data in parallel MRI achieving similarly good reconstruction results as the best sub-space methods.

One question, which still stays to be open regarding the MOCCA approach is to determine a suitable support index set  $\Lambda_L$  for the coil sensitivities in practice. A larger support index set may lead to many singular values of the MOCCA matrix  $\mathbf{A}_M$  in

(3.10) being close to zero. In this case, the choice of a suitable linear combination of singular vectors is crucial to achieve satisfying sensitivities and image reconstructions. In this paper, we have exemplarily shown that the MOCCA algorithm can outperform several other methods, while the problem of finding an optimal linear combination of singular vectors in case of overestimated support set is still under investigation.

There is a close connection between the MOCCA approach and the subspace methods ESPiRiT and SAKE which we study in a forthcoming paper [21]. A better understanding of the relation between subspace methods and sensitivity modelling will help us to answer the question of optimal recovering of sensitivity profiles with small  $k$ -space support and to find other sensitivity models being appropriate for parallel MRI reconstructions thereby still allowing fast reconstruction procedures.

## Acknowledgements

G. Plonka and Y. Riebe acknowledge support by the Deutsche Forschungsgemeinschaft in the CRC 1456, project B03 and by the European Union’s Horizon 2020 research and innovation programme under the Marie Skłodowska-Curie grant agreement No 101008231. Yannick Riebe acknowledges support by the Deutsche Forschungsgemeinschaft in the RTG 2088. The authors thank Benjamin Kocurov and Martin Uecker for helpful discussions.

## References

- [1] M. J. ALLISON, S. RAMANI, AND J. A. FESSLER, *Accelerated regularized estimation of MR coil sensitivities using augmented Lagrangian methods*, IEEE Trans. Med. Imaging, 32 (2013), pp. 556–564.
- [2] K. T. BLOCK, M. UECKER, AND J. FRAHM, *Undersampled radial MRI with multiple coils. Iterative image reconstruction using a total variation constraint*, Magn. Reson. Med., 57 (2007), pp. 1086–1098.
- [3] F. A. BREUER, M. BLAIMER, R. M. HEIDEMANN, M. F. MUELLER, M. A. GRISWOLD, AND P. M. JAKOB, *Controlled aliasing in parallel imaging results in higher acceleration (CAIPiRINHA) for multi-slice imaging*, Magn. Reson. Med., 53 (2005), pp. 684–691.
- [4] Y. CHEN, W. HAGER, F. HUANG, D. PHAN, X. YE, AND W. YIN, *Fast algorithms for image reconstruction with application to partially parallel MR imaging*, SIAM J. Imaging Sci., 5 (2012), pp. 90–118.
- [5] L. FENG, R. GRIMM, K. BLOCK, H. CHANDARANA, S. KIM, J. XU, L. AXEL, D. SODICKSON, AND R. OTAZO, *Golden-angle radial sparse parallel MRI: combination of compressed sensing, parallel imaging, and golden-angle radial sampling for fast and flexible dynamic volumetric MRI*, Magn. Reson. Med., 72 (2014), pp. 707–717.
- [6] R. FENG, Q. WU, J. FENG, H. SHE, C. LIU, Y. ZHANG, AND H. WEI, *IM-JENSE: Scan-specific implicit representation for joint coil sensitivity and image estimation in parallel MRI*, IEEE Trans. Med. Imaging, 43 (2024), pp. 1539–1553.

- [7] J. A. FESSLER, *Optimization methods for magnetic resonance image reconstruction: Key models and optimization algorithms*, IEEE Signal Process. Mag., 37 (2020), pp. 33–40.
- [8] M. GRISWOLD, P. M. JAKOB, R. HEIDEMANN, M. NITTKA, V. JELLUS, J. WANG, B. KIEFER, AND A. HAASE, *Generalized autocalibrating partially parallel acquisitions (GRAPPA)*, Magn. Reson. Med., 47 (2002), pp. 1202–1210.
- [9] J. HALDAR, *Local modeling of local-space neighborhoods (LORAKS) for constrained MRI*, IEEE Trans. Med. Imaging, 33 (2014), pp. 668–681.
- [10] J. HALDAR AND J. ZHUO, *P-LORAKS: Low-rank modeling of local k-space neighborhoods with parallel imaging data*, Magn. Reson. Med., 75 (2016), pp. 1499–1514.
- [11] K. HAMMERNIK, T. KLATZER, E. KOBLER, M. RECHT, D. SODICKSON, T. POCK, AND F. KNOLL, *Learning a variational network for reconstruction of accelerated MRI data*, Magn. Reson. Med., 79 (2018), pp. 3055–3071.
- [12] G. HARIKUMAR AND Y. BRESLER, *Perfect blind restoration of images blurred by multiple filters: theory and efficient algorithms*, IEEE Trans. Image Process., 8 (1999), pp. 202–219.
- [13] R. HEIDEMANN, M. GRISWOLD, A. HAASE, AND P. JAKOB, *VD-AUTO-SMASH imaging*, Magn. Reson. Med., 45 (2001), pp. 1066–1074.
- [14] H. HOLME, S. ROSENZWEIG, F. ONG, R. WILKE, M. LUSTIG, AND M. UECKER, *ENLIVE: An efficient nonlinear method for calibrationless and robust parallel imaging*, Sci. Rep., 9 (2019), p. 3034.
- [15] J. HU, Z. YI, Y. ZHAO, J. ZHANG, L. XIAO, C. MAN, V. LAU, AND A. T. L. LEONG, *Parallel imaging reconstruction using spatial nulling maps*, Magn. Reson. Med., 90 (2023), pp. 502–519.
- [16] Y. HU, W. GAN, C. YING, T. WANG, C. ELDENIZ, J. LIU, Y. CHEN, H. AN, AND U. S. KAMILOV, *SPICER: Self-supervised learning for MRI with automatic coil sensitivity estimation and reconstruction*, Magn. Reson. Med., 92 (2024), pp. 1048–1063.
- [17] M. JACOB, M. P. MANI, AND J. YE, *Structured low-rank algorithms: Theory, magnetic resonance applications, and links to machine learning*, IEEE Signal Process. Mag., 37 (2020), pp. 54–68.
- [18] P. JAKOB, M. GRISWOLD, R. EDELMAN, AND D. SODICKSON, *AUTO-SMASH: a self-calibrating technique for SMASH imaging*, Magn. Reson. Med., 7 (1998), pp. 42–54.
- [19] S. L. KEELING, C. CLASON, M. HINTERMÜLLER, F. KNOLL, A. LAURAIN, AND G. VON WINCKEL, *An image space approach to Cartesian based parallel MR imaging with total variation regularization*, Med. Image Anal., 16 (2012), pp. 189–200.
- [20] F. KNOLL, K. HAMMERNIK, C. ZHANG, S. MOELLER, T. POCK, D. SODICKSON, AND M. AKÇAKAYA, *Deep-learning methods for parallel magnetic resonance imaging reconstruction: A survey of the current approaches, trends, and issues*, IEEE Signal Process. Mag., 37 (2020), pp. 128–140.
- [21] B. KOCUROV AND G. PLONKA, *Mathematical background of MRI subspace methods: ESPIRiT versus MOCCA*, in preparation, (2024).

- [22] E. LARSSON, D. ERDOGMUS, R. YAN, J. PRINCIPE, AND J. FITZSIMMONS, *SNR-optimality of sum-of-squares reconstruction for phased-array magnetic resonance imaging*, J. Magn. Reson., 163 (2003), pp. 121–123.
- [23] D. LEE, K. JIN, E. KIM, S.-H. PARK, AND J. YE, *Acceleration of MR parameter mapping using annihilating filter-based low rank Hankel matrix (ALOHA)*, Magn. Reson. Med., 76 (2016), pp. 1848–1864.
- [24] Y. LI, R. H. CHAN, L. SHEN, X. ZHUANG, R. WU, Y. HUANG, AND J. LIU, *Exploring structural sparsity of coil images from 3-dimensional directional tight framelets for SENSE reconstruction*, SIAM J. Imaging Sci., 17 (2024), pp. 888–916.
- [25] Y.-R. LI, R. H. CHAN, L. SHEN, Y.-C. HSU, AND W.-Y. I. TSENG, *An adaptive directional Haar framelet-based reconstruction algorithm for parallel magnetic resonance imaging*, SIAM J. Imaging Sci., 9 (2016), pp. 794–821.
- [26] R. LOBOS, C.-C. CHAN, AND J. HALDAR, *New theory and faster computations for subspace-based sensitivity map estimation in multichannel MRI*, IEEE Trans. Med. Imaging, 43 (2024), pp. 286–296.
- [27] M. LUSTIG, D. DONOHO, AND J. M. PAULY, *Sparse MRI: The application of compressed sensing for rapid MR imaging*, Mag. Reson. Med., 58 (2007), pp. 1182–1195.
- [28] M. LUSTIG AND J. PAULY, *SPIRIT: Iterative self-consistent parallel imaging reconstruction from arbitrary k-space*, Mag. Reson. Med., 64 (2010), pp. 457–471.
- [29] R. L. MORRISON, M. JACOB, AND M. N. DO, *Multichannel estimation of coil sensitivities in parallel MRI*. 4th IEEE International Symposium on Biomedical Imaging: From Nano to Macro, Arlington, VA, USA, 2007.
- [30] M. J. MUCKLEY, D. C. NOLL, AND J. A. FESSLER, *Fast parallel MR image reconstruction via B1-based, adaptive restart, iterative soft thresholding algorithms (BARISTA)*, IEEE Trans. Med. Imaging, 34 (2015), pp. 578–588.
- [31] M. J. MUCKLEY, B. RIEMENSCHNEIDER, A. RADMANESH, S. KIM, G. JEONG, J. KO, Y. JUN, H. SHIN, D. HWANG, M. MOSTAPHA, S. ARBERET, D. NICKEL, Z. RAMZI, P. CIUCIU, J.-L. STARCK, J. TEUWEN, D. KARKALOUSOS, C. ZHANG, A. SRIRAM, Z. HUANG, N. YAKUBOVA, Y. W. LUI, AND F. KNOLL, *Results of the 2020 fastMRI challenge for machine learning MR image reconstruction*, IEEE Trans. Med. Imaging, 40 (2021), pp. 2306–2317.
- [32] G. PLONKA, *A digital diffusion-reaction type filter for nonlinear denoising*, Results. Math., 53 (2009), pp. 371–381.
- [33] G. PLONKA, D. POTTS, G. STEIDL, AND M. TASCHE, *Numerical Fourier Analysis*, Birkhäuser, Cham, 2nd ed., 2023.
- [34] K. PRUESSMANN, M. WEIGER, M. SCHEIDECKER, AND P. BOESIGER, *SENSE: sensitivity encoding for fast MRI*, Magn. Reson. Med., 42 (1999), pp. 952–962.
- [35] S. RAMANI AND J. A. FESSLER, *Parallel MR image reconstruction using augmented Lagrangian methods*, IEEE Trans. Med. Imaging, 30 (2011), pp. 694–706.
- [36] H. SHE, R.-R. CHEN, D. LIANG, Y. CHANG, AND L. YING, *Image reconstruction from phase-array data based on multichannel blind deconvolution*, Magn. Reson. Imaging, 33 (2015), pp. 1106–1113.

- [37] J. SHENG, E. WIENER, B. LIU, F. BOADA, AND L. YING, *Improved self-calibrated spiral parallel imaging using JSENSE*, Med. Eng. Phys., 31 (2009), pp. 510–514.
- [38] P. SHIN, P. E. Z. LARSON, M. A. OHLIGER, M. ELAD, J. M. PAULY, D. B. VIGNERON, AND M. LUSTIG, *Calibrationless parallel imaging reconstruction based on structured low-rank matrix completion*, Magn. Reson. Med., 72 (2014), pp. 959–970.
- [39] D. SODICKSON AND W. MANNING, *Simultaneous acquisition of spatial harmonics (SMASH): fast imaging with radiofrequency coil arrays*, Magn. Reson. Med., 38 (1997), pp. 591–603.
- [40] P. SURYANARAYANA, P. PRATAPA, AND J. PASK, *Alternating Anderson–Richardson method: An efficient alternative to preconditioned Krylov methods for large, sparse linear systems*, Comput. Phys. Commun., 234 (2019), pp. 278–285.
- [41] M. UECKER, T. HOHAGE, K. BLOCK, AND J. FRAHM, *Image reconstruction by regularized nonlinear inversion-joint estimation of coil sensitivities and image content*, Magn. Reson. Med., 60 (2008), pp. 674–682.
- [42] M. UECKER, P. LAI, M. J. MURPHY, P. VIRTUE, M. ELAD, J. PAULY, S. VASANAWALA, AND M. LUSTIG, *ESPIRiT—an eigenvalue approach to autocalibrating parallel MRI: Where SENSE meets GRAPPA*, Magn. Reson. Med., 71 (2014), pp. 990–1001.
- [43] M. UECKER AND M. LUSTIG, *Estimating absolute-phase maps using ESPIRiT and virtual conjugate coils*, Magn. Reson. Med., 77 (2017), pp. 1201–1207.
- [44] S. WANG, H. CHENG, L. YING, T. XIAO, Z. KE, H. ZHENG, AND D. LIANG, *DeepcomplexMRI: Exploiting deep residual network for fast parallel MR imaging with complex convolution*, Magn. Reson. Imaging, 68 (2020), pp. 136–147.
- [45] L. YING AND J. SHENG, *Joint image reconstruction and sensitivity estimation in SENSE (JSENSE)*, Magn. Reson. Med., 57 (2007), pp. 1196–1202.
- [46] J. ZHANG, C. LIU, AND M. E. MOSELEY, *Parallel reconstruction using null operations*, Magn. Reson. Med., 66 (2011), pp. 1241–1253.